FIRST-PRINCIPLES DESIGN OF HYBRID CARBON NITRIDE (C_2N) WITH GALLIUM SULPHIDE AND GALLIUM SELENIDE TWO-DIMENSIONAL (2D) MATERIALS AS HIGH-PERFORMANCE PHOTOVOLTAIC CELLS

By

SEISO EMMANUEL TSOEU

Student number: 201112236

Dissertation in fulfilment of the requirement for the degree

MASTERS IN SCIENCE

In

CHEMISTRY

In the

FACULTY OF SCIENCE

Of the

UNIVERSITY OF JOHANNESBURG

Supervisor: PROF PP GOVENDER

Co-supervisor: DR F OPOKU

Jan 2021

DECLARATION

I hereby declare that this dissertation, which I herewith submit for the research qualification

MASTERS IN CHEMISTRY

To the University of Johannesburg, Department of Chemical Sciences, is, apart from the recognised assistance of my supervisors, my work and has not previously submitted by me to another institution to obtain a research degree.

Mr Seiso Emmanuel Tsoeu _____ on this _08_day of January_2021

(Candidate)

Prof Penny Poomani Govender _ _ on this _08__day of _January 2021

(Supervisor)

Dr Francis Opoku _____ on this _08__ day of_ January_2021

(Co-supervisor)

DEDICATION

My Parents (Mr Hlalele Mabathoana & Mrs Morogoe Tsoeu)

Strong and gentle souls that taught me to trust in God, believe in hard work and that so much could be achieved with little you have.

My Grandparents (Mrs Mahlalele Mabathoana & Mrs Malehloa Tsoeu)

Whatever I put out in this world, it will come back to me ten-fold good or bad. I am very grateful for the guidance you both given me.

To All Mabathoana Clan

Having somewhere to go is Home. Having someone to love is a family. Having both is a blessing.

To All Tsoeu Clan

Being a family means you are part of something very delightful. The gift I got from this family.

"*Ke Mohlakoana oa mapholo ea lisema maila ngoatheloa,*

Motho ea sajeng sengoathoana sa maobane,

Motho ea reng haja ho thehe merithi,

Hothehe le e menyenyane ea liotloana,

Motho ea sa janeng polokoe kaofela…"

PUBLICATIONS AND PRESENTATIONS

The work presented in this thesis has been presented at national and international conferences. Furthermore, results emanating from this study have also been either published or submitted to peer-reviewed journals. List below:

Presentations

1. S.E Tsoeu, Opoku F, Govender P.P "*Tuning the electronic, optical and structural properties of two-dimensional GaS/C_2N van der Waals heterostructure for photovoltaic application: First-principle Calculations*" 13th Centre for High-Performance Computing National Conference, Birchwood Conference Centre, Boksburg, Johannesburg, 2nd – 4th December 2019.
2. S.E Tsoeu, Opoku F, Govender P.P "*Tuning the electronic, optical and structural properties of two-dimensional GaS/C_2N van der Waals heterostructure for photovoltaic application: First-principle Calculations*" PG Research day, University of Johannesburg - 6th – 8th November 2019.

Publications

1. S.E Tsoeu, Opoku F, Govender P.P. (2020). *Tuning the electronic, optical and structural properties of two-dimensional GaS/C_2N van der Waals heterostructure for photovoltaic application: First-principle Calculations*. SN Applied Sciences. *DOI.org/10.1007/s42452-020-2091-y*
2. S.E Tsoeu, Opoku F, Govender P.P. (2020). *Exploring the optical, structural and electronic properties of two-dimensional GaSe/C_2N van der Waals heterostructure as photovoltaic cell: A computational investigation*. Journal of Electronic Materials. *DOI 10.1007/s11664-020-08606-9*

ACKNOWLEDGEMENTS

Genuine gratitude to the accompanying individuals and foundations for their help: The financial contributions from the Faculty of Science; Centre for Nanomaterials Science Research, University of Johannesburg, South Africa; and the National Research Foundation South Africa (TTK170405225933). Also, grateful to the National Integrated Cyber Infrastructure System (NICIS) and Centre for High-Performance Computing, Cape Town, South Africa, for allowing the use of the cluster/facilities throughout the study.

I am thankful for the following people who have provided me with motivation, help, inspiration and proper guidance that was needed to complete this project:

- Prof Penny P. Govender - Department of Chemical Sciences, University of Johannesburg, Doornfontein Campus, Johannesburg, Gauteng, South Africa.
- Dr Francis Opoku - Department of Chemical Sciences, University of Johannesburg, Doornfontein Campus, Johannesburg, Gauteng, South Africa.

Special thanks to Dr Krishna Kuben Govender from CHPC for valuable inputs and always available for any incurred problems I faced during my work on the cluster. I am exceedingly grateful to the Computational Chemistry and Experimental research group members (Dr Ephraim Felix Marondedze, Dr Renu Kumari, Dr Wahab Olaide, Mr Ephraim Muriithi Kiarii, Dr William Wilson Anku, Dr Adeniyi Osikoya, Mrs Nokuthula Ndaba, Mr Sechaba Mayedi, Mr Elvis Ahiahonu, Miss Reitumetse Molefi, Mr Solomon Pole and Mr Michael Kumi). Lastly, a special thanks to the

administrators (Ms Leah Moshe, Mr Sifiso Tshabalala, Mrs Dereshni Ramnarain and Mrs Dorcas Babupi) in the Department of Chemical Sciences; your assistance will always be appreciated.

THANK YOU AND MAY GOD BLESS YOU!

ABSTRACT

The high demand for renewable energy has been imperative for the source of energy. Following the global energy market, fossil fuels as non-renewable natural resources cannot be viable and will be lost over the years. The photovoltaic cell is renewable and can be harnessed using two-dimensional (2D) semiconductors. This helps in less contamination and green energy generation. However, 2D materials have been used to absorb maximum visible light and convert solar energy directly into electricity, where C_2N has a promising application due to its economic affordability, chemical stability, earth-abundant nature, high thermal and tunable electronic structure. Heterostructure formation was designed to address the rapid recombination of charge carriers of C_2N sheets.

The results presented in this dissertation were obtained using density functional theory within the Cambridge Serial Total Energy Package package (CASTEP). A theoretical bandgap of 1.960, 1.953, 2.376 and 2.050 eV was calculated for C_2N sheet, C_2N sheet, GaS monolayer and GaSe monolayer, respectively. Both GaS/C_2N and GaSe/C_2N heterostructures showed a bandgap of 1.251 and 1.357 eV, respectively. The heterostructures showed a low work function compared to GaS, GaSe and C_2N sheet. The reduced bandgap of GaS/C_2N and GaSe/C_2N heterostructures suggest a high charge transfer, making C_2N sheet receive electrons from GaS and GaSe monolayers. The calculated band edges of GaS/C_2N heterostructure exhibited type-I alignment, while GaSe/C_2N heterostructure exhibited type-II alignment.

The calculated power conversion efficiency of GaS/C_2N and $GaSe/C_2N$ heterostructures show a relatively high conversion of 17.8 and 21.2%, respectively. We proposed that GaS/C_2N and $GaSe/C_2N$ heterostructures could exhibit photo-stability, enhanced visible light absorption and better transfer of photogenerated charge carriers. The overall theoretical studies could be valuable for designing photovoltaic cells.

TABLE OF CONTENTS

LIST OF FIGURES AND SCHEMATICS

LIST OF TABLES

LIST OF ABBREVIATIONS

1G	First Generation
2G	Second Generation
3G	Third Generation
4G	Fourth Generation
2D	Two Dimensional
ARF	Anti-Reflecting Film
C_2N	Carbon Nitride
CASTEP	Cambridge Serial Total Energy Package
CB	Conduction Band Minimum
DFT	Density Functional Theory
DSSC	Dye-Sensitized Solar Cells
FF	Fill Factor
FTO	Fluorine doped Tin Oxide
GaS	Gallium Sulphide
GaSe	Gallium selenide
GGA	Generalized Gradient Approximation
GW	Gigawatt
HSE06	Heyd-Scuseria-Ernzerhof

IPCE	Incident Photo-to-Current Efficiency
J_{sc}	Short-Circuit Current
NIR	Near-Infrared
NREL	National Renewable Energy Laboratory
OPV	Organic Photovoltaic Cell
PBE	Perdew-Burke-Ernzerhof
PCE	Power Conversion Efficiency
PDOS	Potential Density of States
PSC	Polymer Solar Cell
PV	Photovoltaic Cell
Si	Silicon
TiO_2	Titanium Dioxide
TSC	Transparent Solar Cell
TPV	Thin-film Photovoltaic Cell
TLSC	Transparent Luminescent Solar Concentrator
UV	Ultraviolent
VBM	Valence Band Maximum
V_{oc}	Open-Circuit Voltage

CHAPTER 1:

INTRODUCTION

1.1 Background

Energy is one of the essential tools to sustain life. The demand for energy in the world has become a serious matter, as the human population is continuously increasing. Therefore, more energy and attractive sources of energy are needed. Industries use non-renewable resources to generate energy that contributes to the greenhouse effect. The Photovoltaic (PV) process is a promising new technology for generating clean and sustainable energy. Photovoltaic generates electricity by converting solar energy radiation into a direct electric current using semiconductor materials [1]. The photovoltaic process has become a significant focus of energy generation because of its great advantages, such as low costs and being environmentally-friendly [1, 2]. The PV process occurs when photons of light from the solar energy excite electrons of the semiconductor to a higher energy state/conduction band minimum (CBM) from a lower energy state/valence band maximum (VBM) and as a result, an electric current is generated [3].

The PV cell built with a thin layer of monocrystalline silicon (Si) semiconductor [4] converts energy from sunlight into useful electrical energy [5]. Since Si was the first semiconductor used in first-generation (1G) PV cells, therefore, about 80% of the PV cell panels are built with Si [6]. The 1G semiconductor reported high-efficiency of absorbing PV energy, but purifying Si makes the tenability of electronic-grade crystalline Si to be more costly [7]. This has led to the search of second-generation (2G) PV cells, such as cadmium telluride (CdTe), amorphous silicon and copper indium gallium diselenide thin-film semiconductors. However, the 2G PV cells provide

a low efficiency than 1G cells [1]. The third-generation (3G) consisting of organic materials, such as polymers, two-dimensional and organic dyes were made to measure the cost and increase the efficiency of the materials [2]. Lately, ongoing investigations on the fourth generation (4G) comprising inorganic-organic materials for PV cells are underway [3, 4]. The 4G main focus is on linking the advantages of both organic and inorganic nanomaterials. This is mainly due to organic materials that have a low cost to manufacture, easy to process, and physically flexible, whereas the inorganic materials have high charge transfer, higher stability, and dissociation [3]. The combination of 3G and 4G properties with both their advantages focus on the efficiency of photovoltaic technologies [4].

The modern PV cells were built on the principle of electron-hole pairs, having a negative side (n-type semiconductor layer) and a positive side (p-type semiconductor layer), allowing a flow of electrons (e^-) with a connection wire to form a circuit [5]. The n-type semiconductor layer is stacked on top of the p-type semiconductor layer, where a photon from the sun strikes the cell, which causes sufficient energy to dislodge an electron from the p-type layer to the n-type layer [6]. The energized electron will be N circuit, electrons will flow within a wire to generate electrical energy.

Currently, several semiconductor materials are being developed to generate electrical energy for industries and household usage. The use of two-dimensional (2D) materials is popular due to its high charge carrier mobility [7], superconductivity [8] and excellent thermal conductivity [9], as well as high optical properties [10]. The 2D-based heterostructures are used to increase the performance of photovoltaic materials, allowing a substantial reduction in the physical width of photovoltaic absorber layers [11]. Carbon nitride (C_2N) has been studied theoretically and experimentally, revealing

the most significant potential for the photovoltaic process due to its unique electrical and optical properties [12], tunable electronic structure [13], chemical stability [14] and nanowire electronic [15]. C_2N semiconductor shows the suitable character of electrical conversion [16] and has phonon modes close to graphene [17].

C_2N contains N-rings and similar porous structures to g-C_3N_4 (graphitic-carbon nitride) [18, 19] where the nitrogenized holes are formed in an ordered pattern of a triangle. The C_2N structure is confirmed to have a direct band-gap semiconductor character with an optical bandgap energy of 1.96 eV [20]. It has been successfully prepared experimentally by a bottom-up wet chemical reaction and applied in photocatalysis [21] and photovoltaic processes [22, 23] for water purification and electricity generation, respectively.

Other 2D materials, such as gallium sulphide (GaS) and gallium selenide (GaSe) structures, have attracted a lot of attention in the field of the photovoltaic process [24, 25]. The experimental work of synthesizing GaS and GaSe nanosheets have been successfully carried out [26]. The structures of GaS and GaSe consists of four covalent bond atoms stacked vertically to each other as X-Ga-Ga-X (X = S or Se), by weak van der Waal forces [27, 28], as shown in Figure 1.1(a-d).

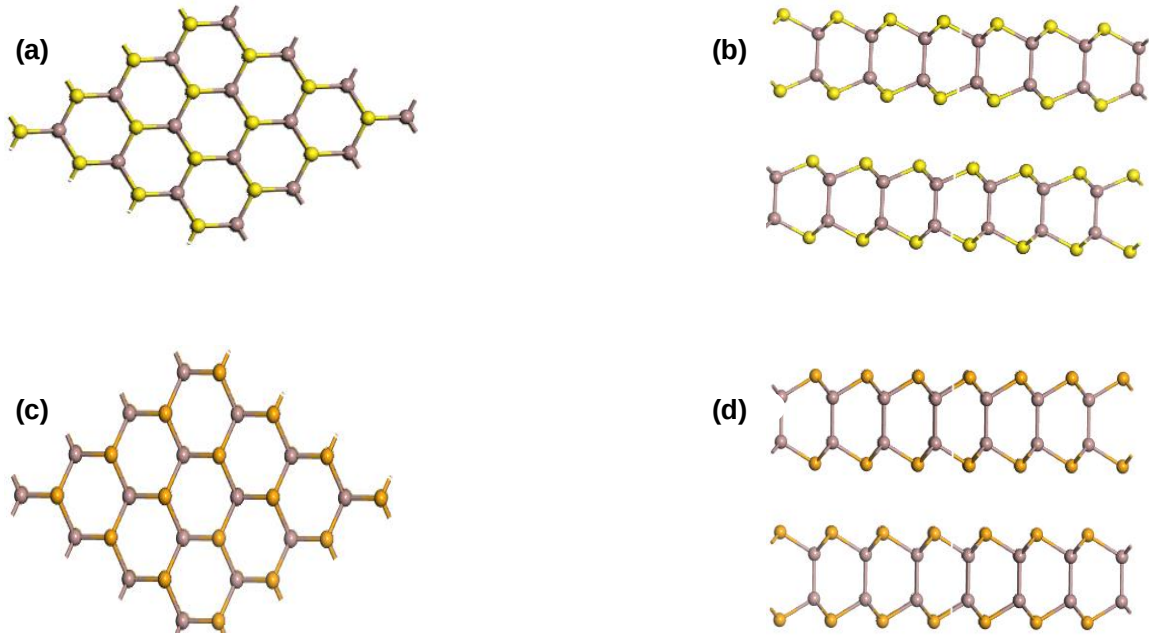

Figure 1.1. (a-b) GaS structures and (c-d) GaSe structures.

1.2 Problem Statement

More than 80% of global energy demand is supplied by the burning of fossil fuels, which releases greenhouse gases causing global warming. The development of alternative renewable energy sources to replace traditional fossil fuels is important to achieve sustainability and clean energy carrier resources. Solar energy is vital and clean for future energy. The photovoltaic process has received considerable attention due to its widespread use that can decrease the cost of electricity generation and is also environmentally friendly.

The problem of matching electric power supply with demand is continuously faced by power systems in South Africa and the whole world in general. The demand growth is slow in industrialized countries in recent years, but energy shortages still occur in developing countries [29]. Electricity is expected to increase its global share of the

supplied energy market and plans to meet potential demands for electricity from economically and environmentally appropriate sources necessary for development. The current position of the supply of electricity is still facing problems; therefore, the search for alternative ways of generating renewable energy using methods, such as wind, wave, photovoltaic cells and hydropower to solve the problems is ongoing [29].

In this work, photovoltaic cells are carefully considered and factors that promote the photovoltaic efficiency such as enhanced charge carrier separation and transfer, suitable bandgap energy and excellent optical properties are studied. Density Functional Theory (DFT) method has been used to study the electronic and structural properties of materials since it can address the effects of electron correlation by accounting for inter-electron interactions [30]. Despite the high surface area, excellent thermo-stability and a similar structure, such as g-C_3N_4, the rapid recombination rate of photo-induced charge carriers limit the photovoltaic application of C_2N sheet.

Combining C_2N sheet with different semiconductor materials containing different band gaps and electron affinity to form a heterostructure can enhance the charge carrier separation and transfer of C_2N sheet, thereby increasing the photosensitivity absorption in the detectable region of solar energy [31]. In this study, C_2N is stacked with GaS and GaSe dichalcogenides to form heterostructure and decrease the bandgap of any photovoltaic material. Besides, the importance of heterostructure can decrease the bandgap of any photovoltaic material, where some charge carriers are produced when a visible light excites electrons of the PV cell [32]. Earlier studies revealed that heterostructure materials can decrease the bandgap energy of a C_2N sheet and increase the photosensitive fascination in the detectable area of solar

energy [33]. The lower effective mass of charge carriers helps an effective charge separation in the heterostructure [31].

1.3 Aim and Objectives

1.3.1 Aims

The project aims to design a photovoltaic material that can be used to generate energy by forming heterostructures based-on 2D materials.

1.3.2 Objectives

In this research, we aim to:

1. Design GaS/C_2N heterostructure and $GaSe/C_2N$ heterostructure materials, which can be used as photovoltaic cells.
2. Determine the formation energy, optical, electronic and structural properties of GaS/C_2N heterostructure and $GaSe/C_2N$ heterostructure materials.
3. Test the optimal performance and catalytic stability of the proposed materials.
4. Gain fundamental insights into the mechanism of the improved photovoltaic performance of the predicted GaS/C_2N heterostructure and $GaSe/C_2N$ heterostructure materials.

1.4 Outline of the thesis

The dissertation is prepared as follows:

Chapter 1 contains the background information of materials used and their individual properties, problem statement, aim and objectives.

Chapter 2 contains the nature and the origin of the photovoltaic cell with different PV cells that have been developed. It further explains the semiconductors used in this study.

Chapter 3 describes the theoretical methods performed in this work and the tools with their information.

Chapter 4 is about tuning the electronic, optical and structural properties of GaS/C_2N van der Waals heterostructure for photovoltaic application: First-Principles calculations. The obtained results have been published in a peer-review journal.

Chapter 5 explores the optical, structural and electronic properties of two-Dimensional $GaSe/C_2N$ van der Waals Heterostructure for photovoltaic devices: computational Investigation.

Chapter 6 is the conclusion and recommendation of the research.

1.5 References

[1] O. Vigil-Galán, M. Courel, J. Andrade-Arvizu, Y. Sánchez, M. Espíndola-Rodríguez, E. Saucedo, D. Seuret-Jiménez and M. Titsworth. Route towards low cost-high efficiency second generation solar cells: current status and perspectives. *J. Mater. Sci.: Mater. Electron.* **26** (2015) 5562-5573.

[2] A. L. Bristow, M. Tight, A. Pridmore and A. D. May. Developing pathways to low carbon land-based passenger transport in Great Britain by 2050. *Energy Policy* **36** (2008) 3427-3435.

[3] K. I. Jayawardena, L. J. Rozanski, C. A. Mills, M. J. Beliatis, N. A. Nismy and S. R. P. Silva. 'Inorganics-in-Organics': recent developments and outlook for 4G polymer solar cells. *Nanoscale* **5** (2013) 8411-8427.

[4] T. P. Nguyen and J. H. Shim. Hybrid density functional study on the electronic structures and properties of P3HT-PbS and P3HT-CdS hybrid interface for photovoltaic applications. *J. Comput. Chem.* **39** (2018) 1990-1999.

[5] T. M. Razykov, C. S. Ferekides, D. Morel, E. Stefanakos, H. S. Ullal and H. M. Upadhyaya. Solar photovoltaic electricity: Current status and future prospects. *Sol. Energy* **85** (2011) 1580-1608.

[6] B. Srinivas, S. Balaji, M. Nagendra Babu and Y. Reddy. Review on present and advance materials for solar cells. *Int. J. Eng. Res-online.* **3** (2015) 178-182.

[7] K. I. Bolotin, K. J. Sikes, Z. Jiang, M. Klima, G. Fudenberg, J. Hone, P. Kim and H. Stormer. Ultrahigh electron mobility in suspended graphene. *Solid State Commun.* **146** (2008) 351-355.

[8] I.-W. Chung, S.-J. Kwon, S.-J. Kim, E. S. Jang, S.-J. Hwang and J.-H. Choy. Evidence of two-dimensional superconductivity in the single crystalline

nanohybrid of organic-bismuth cuprate. *J. Phy. Chem. B* **110** (2006) 16197-16200.

[9] Z.-S. Wu, W. Ren, L. Gao, J. Zhao, Z. Chen, B. Liu, D. Tang, B. Yu, C. Jiang and H.-M. Cheng. Synthesis of graphene sheets with high electrical conductivity and good thermal stability by hydrogen arc discharge exfoliation. *ACS Nano* **3** (2009) 411-417.

[10] L. Song, L. Ci, H. Lu, P. B. Sorokin, C. Jin, J. Ni, A. G. Kvashnin, D. G. Kvashnin, J. Lou and B. I. Yakobson. Large scale growth and characterization of atomic hexagonal boron nitride layers. *Nano Lett.* **10** (2010) 3209-3215.

[11] M. Graetzel, R. A. Janssen, D. B. Mitzi and E. H. Sargent. Materials interface engineering for solution-processed photovoltaics. *Nature* **488** (2012) 304-312.

[12] J. Mahmood, E. K. Lee, M. Jung, D. Shin, I.-Y. Jeon, S.-M. Jung, H.-J. Choi, J.-M. Seo, S.-Y. Bae and S.-D. Sohn. Nitrogenated holey two-dimensional structures. *Nat. Commun.* **6** (2015) 1-7.

[13] Y. Wang, N. Song, M. Jia, D. Yang, C. Panashe, Y. Yang and J. Wang. Tunable electronic structure and magnetic moment in C_2N nanoribbons with different edge functionalization atoms. *Phys. Chem. Chem. Phys.* **19** (2017) 15021-15029.

[14] A. Pakdel, Y. Bando and D. Golberg. Nano boron nitride flatland. *Chem. Soc. Rev.* **43** (2014) 934-959.

[15] Y. Li, F. Qian, J. Xiang and C. M. Lieber. Nanowire electronic and optoelectronic devices. *Mater. Today* **9** (2006) 18-27.

[16] M. Ashwin Kishore and P. Ravindran. Tailoring the electronic band gap and band edge positions in the C_2N monolayer by P and As substitution for photocatalytic water splitting. *J. Phys. Chem. C* **121** (2017) 22216-22224.

[17] W.-J. Ong, L.-L. Tan, Y. H. Ng, S.-T. Yong and S.-P. Chai. Graphitic carbon nitride ($g\text{-}C_3N_4$)-based photocatalysts for artificial photosynthesis and environmental remediation: Are we a step closer to achieving sustainability? *Chem. Rev.* **116** (2016) 7159-7329.

[18] D. Ma, Q. Wang, X. Yan, X. Zhang, C. He, D. Zhou, Y. Tang, Z. Lu and Z. Yang. 3d transition metal embedded C_2N monolayers as promising single-atom catalysts: a first-principles study. *Carbon* **105** (2016) 463-473.

[19] B. He, J. Shen and Z. Tian. Iron-embedded C_2N monolayer: a promising low-cost and high-activity single-atom catalyst for CO oxidation. *Phys. Chem. Chem. Phys.* **18** (2016) 24261-24269.

[20] J. Mahmood, E. K. Lee, M. Jung, D. Shin, I.-Y. Jeon, S.-M. Jung, H.-J. Choi, J.-M. Seo, S.-Y. Bae and S.-D. Sohn. Nitrogenated holey two-dimensional structures. *Nature commun.* **6** (2015) 1-7.

[21] H. Wang, X. Li and J. Yang. The $g\text{-}C_3N4/C_2N$ Nanocomposite: A $g\text{-}C_3N_4$-Based Water-Splitting Photocatalyst with Enhanced Energy Efficiency. *Chem. Phys. Chem.* **17** (2016) 2100-2104.

[22] S. E. Shaheen, D. S. Ginley and G. E. Jabbour. Organic-based photovoltaics: toward low-cost power generation. *MRS Bull.* **30** (2005) 10-19.

[23] D. Jariwala, A. R. Davoyan, J. Wong and H. A. Atwater. Van der Waals materials for atomically-thin photovoltaics: Promise and outlook. *Acs Photonics* **4** (2017) 2962-2970.

[24] J. Dries Schottky barriers on the layer compound gallium-sulphide (1977)

[25] Z. Liu, Q. Liu, Y. Huang, Y. Ma, S. Yin, X. Zhang, W. Sun and Y. Chen. Organic photovoltaic devices based on a novel acceptor material: graphene. *Adv. Mater.* **20** (2008) 3924-3930.

[26] P. Hu, Z. Wen, L. Wang, P. Tan and K. Xiao. Synthesis of few-layer GaSe nanosheets for high performance photodetectors. *ACS Nano.* **6** (2012) 5988-5994.

[27] T. Wieting and J. Verble. Infrared and Raman Investigations of Long-Wavelength Phonons in Layered Materials. in Electrons and phonons in layered crystal structures. Springer, (1979), 321-407.

[28] L. Huang, Z. Chen and J. Li. Effects of strain on the band gap and effective mass in two-dimensional monolayer GaX (X= S, Se, Te). *RSC Adv.* **5** (2015) 5788-5794.

[29] M. John. Electricity supply-problems and possibilities. *Electron. Power* **29** (1983) 702-704.

[30] J. Foresman and E. Frish. Exploring chemistry. *Gaussian Inc., Pittsburg, USA* (1996)

[31] J. Mahmood, F. Li, S.-M. Jung, M. S. Okyay, I. Ahmad, S.-J. Kim, N. Park, H. Y. Jeong and J.-B. Baek. An efficient and pH-universal ruthenium-based catalyst for the hydrogen evolution reaction. *Nat. Nanotechnol.* **12** (2017) 441-446.

[32] J. Wang, J. Meng, Q. Li and J. Yang. Single-layer cadmium chalcogenides: promising visible-light driven photocatalysts for water splitting. *Phys. Chem. Chem. Phys.* **18** (2016) 17029-17036.

[33] X. Wang, R. Quhe, W. Cui, Y. Zhi, Y. Huang, Y. An, X. Dai, Y. Tang, W. Chen and Z. Wu. Electric field effects on the electronic and optical properties in C_2N/Sb van der Waals heterostructure. *Carbon* **129** (2018) 738-744.

CHAPTER 2:

LITERATURE REVIEW

2.1 Introduction

The photovoltaic (PV) cell was first discovered in 1839 by Becquerel while busy studying the light effect on electrolytic cells [1]. The group II-VI and III–V semiconductors as PV cell materials were investigated in the early years of the 1960s to provide a very high fabrication capacity at decreasing material consumption and increase input in the production process as well as consequently reduce the cost for large-scale applications for PV cells [2]. The energy crisis of the 1970s motivated the research and development of PV cells.

The PV cells face the challenges of efficiency, cost-effectiveness and operating lifetime of PV cell [3]. Researchers continue to focus on finding suitable materials to overcome the aforementioned challenges of the photovoltaic cell [4]. Although silicon (Si) was found to exhibit an excellent solar energy efficiency of 6% compared to other materials, its high operational costs limit its industrial application [5]. This leads to the need to search for new materials that can offer high solar efficiency with a lower operating cost.

2.1.1 Dye-Sensitized Solar Cells (DSSC): Operational Principal

Dye-sensitized solar cell is one of the designed solar cells that were developed in the early years. O'Regan and Grätzell discovered the manufacturing of dye-sensitized solar cells (DSSC) in early 1991, reporting power efficiency of 7-8%, which was an improvement from monocrystalline silicon as PV cells [6]. DSSC is a

promising energy-generating cell due to their low cost and high power conversion efficiency (PCE). Thus, DSSC materials have attracted a lot of attention over the years [7]. The DSSC has shown the most significant promise as a cheap alternative method to the conventional positive-negative (p-n) junction for solar cells [8]. Highly efficient photovoltaic conversions come from the easy low production costs and manufacturing of the DSSC, making DSSC an interesting technology for large-scale solar energy conversion [9].

The association of a highly porous nanocrystalline TiO_2 film is among the fundamental concepts for developing the DSSC solar cells, enhanced by a light-scattering coat in recent designs. DSSC is a high molar extinction coefficient of dyeing as a sensitizer to form the working electrode of solar cells [9]. The TiO_2 film processing uses nanocrystalline and submicron-crystalline-TiO_2 film screen printing techniques and chemical bath deposition for $TiCl_4$ treatment [10]. A transparent nanocrystalline TiO_2 film combination with a microcrystalline light-scattering layer in conjunction with an anti-reflecting film (ARF), enhances the incident photon-to-electricity current efficiency (IPCE), also known as the external quantum efficiency [10].

2.1.2 Transparent Solar Cell (TSC) Technologies

Transparent solar cell technology was developed to enhance the efficiency of solar energy and different technologies applied to fabricate transparent solar cells. About nine technologies contributed to the manufacturing of transparent solar cells [11].

2.1.2.1 Thin-Film Photovoltaic (TPVs) Technology

Thin-film photovoltaics (TFVs) has been regarded as one of the most productive technologies in TSC. Some of the methods depend mostly on the fabrication of the material and pastes to achieve transparency and others depend specifically on the deposition method of pastes on Fluorine-doped Tin Oxide (FTO) glass [11]. Thin-film photovoltaic is a thin-film with a thickness ranging from a few nanometers to about 10 micrometres [12]. Thin-film reduces the manufacturing costs of solar cells, by using low-cost materials for solar cells. Moreover, it is much easier to deposit TPV on different layers from insulators to metals and rigid to flexible used in several applications [13].

The TPV was fabricated by small particles, which increase the surface area of thin-film and allowing more dye absorption [14]. Introducing smaller particles in TPV did not improve the performance of PV due to the recombination of the electrons that requires an outstanding balance when choosing PV materials [14]. TPV reported an efficiency ranging between 7.8 and 8.4% for 6 and 12μm thickness, respectively, for nano-crystalline films, where both films had a total transmission ranging between 20 and 23% over the wavelength of 400-700 nm [14]. However, this result was unsatisfactory thus leading towards the improvement of the methods.

2.1.2.2 Near-Infrared Transparent Solar Cell

The focus of the transparency technologies is to allow the photons to pass through, making it hard to include both features in the material. Research now focuses on creating a thin layer that achieves a high degree of transparency and absorbs the visible spectrum. The research group of Richard Lupin in 2011 took a different approach by changing the molecules of the dye to absorb ultraviolet and near-

infrared (NIR) wavelengths (650-850 nm) rather than focusing on the thickness of the active layers to accomplish a transparent solar cell [15]. An organic heterojunction PV (OPV) is transparent to visible light with more than 65% transmission and will absorb with an efficiency of 1.3 ± 0.1 in the near-infrared spectrum [15]. The main objective of the TSC model is to permit visible light to pass through and adsorb ultraviolet and near-infrared (NIR) wavelength.

2.1.2.3 Polymer Solar Cell (PSC)

In 2012, a group of researchers investigated the possibilities of PSC using suitable solutions for processing [16]. The absorbing materials should harvest the efficient light in the NIR and ultraviolet (UV) region to allow the visible light to pass through [16]. Two-dimensional carbon-based materials like graphene are promising PSC materials, due to their ability to trap visible light [17]. These materials were also not efficient enough to achieve high solar energy conversion efficiency [18, 19]. This requires a combination of transparent polymers solar cell and conducting material, such as silver nanowires (AgNWs) linked with a transparent polymeric PV cell, which is not transparent to NIR and UV light but transparent to visible light [19]. The polymer solar cell has an efficiency of 4% and the transparency at 550 nm wavelength was about 66% [11]. An efficiency of 7.56% and the average transmission of about 25% was reported. The solar cell structure combines five layers that harvest a region in the visible light spectrum to shelter the entire wavelength [16].

2.1.2.4 Transparent Luminescent Solar Concentrator (TLSC)

TLSC was another developed approach in 2014, which was developed based on organic salts. This takes another direction to realize a new PV cell with an altered

structure, which combines efficiency with transparency [20]. TLSC was developed from luminescent blends of cyanine salts and canine, and it was synthesised from cyanine salts-host blend with the quantum yields, connecting with selective NIR harvesting. The TLSC solar exhibited 86% transparency and achieved an efficiency of 0.4% [20].

2.1.2.5 Perovskite Solar Cell

Researchers are recently focusing on the semi-transparent nature of organic PV cells by utilizing absorbing material having the lowest bandgap than those that can absorb photons. Thus the perovskite cells allow absorption in the near-infrared and visible light region [20].

When focusing on the improvement of transparency, efficiency is also affected positively. This limitation has shifted the focus of finding a transparent material that will improve the PV cell efficiency [21]. The perovskite materials are abundant organic materials with high absorption efficiency, high stability, high carrier mobility, direct bandgap and suitable electric properties [21]. The perovskite crystal structure used in solar cells can achieve a power conversion efficiency as high as 13.0%, making perovskites good materials compared with dye-sensitized solar cells. The power conversion of perovskite solar cells has rapidly increased and recently reached 22.1% [22]. This has led researchers to investigate more on lead-free halide perovskite materials due to the toxic nature of lead used in the inorganic-organic perovskite structures.

The photovoltaic process occurs when the semiconductor material absorbs light/photons, separating electron-hole pairs in one direction accordingly. The used

semiconductor consists of a p-n junction with the potential difference, which later will generate current flowing through the connected cell in one direction. One of the important factors that affect a photovoltaic cell's efficiency is efficient electrons transfer, which can then drive the reduction reaction of the system [23]. In principle, photovoltaic cells are devices that convert sunlight into direct electricity using semiconductor materials. Photovoltaics are applied in several applications: agricultural greenhouse, wastewater, batteries and Bos other components and module temperature distribution.

Photovoltaic energy is based on the photovoltaic effect [24]. Photovoltaic can be used at any available scale, from small electronic appliances to bigger household systems and powerful industrial installations [25]. Photovoltaic is a clean and renewable energy source compared to the traditional way of producing electricity because it is free from releasing greenhouse gases, leading to global warming and adverse effects on human health [26]. To achieve sustainable energy production, the development of PV renewable energy to replace the traditional way is important.

2.2 Photovoltaic Materials

Semiconductors are used to design a well stable and efficient photovoltaic cell by absorbing emitted photons from the sun that will enhance charge separation and migration of electrons. Several criteria are needed to design PVs:

1. The semiconductor bandgap must be enough for harvesting light energy ranging between 1.1-1.5 eV [27, 28] for photovoltaic applications.
2. High charge carrier mobility and/or migration, exciton generation of electrons and chemical stability.

3. The high-energy conversion efficiency of semiconductor materials must possess great potential for high-performance photovoltaic devices.
4. Semiconductors must be earthly-abundant, eco-friendly and low-cost during the manufacturing process through the use of green procedures that meet the global sustainable requirements.

2.2.1 Charge Carrier Generation in Semiconductors

In semiconductors, both electrons and holes are accountable for charge transfer within the semiconductor. The negative charge carriers (electrons) fill up the conduction band and positive charge carriers (holes) fill up the valence bands. The carrier generation does take place with the effect of visible light and the surface of the material, giving electrons enough energy to move from the valence band (VB) to the conduction band (CB). The VB of any semiconductor is the highest occupied molecular orbital (HOMO), whereas the CB is composed of the lowest unoccupied molecular orbital (LUMO) [29, 30]. The energy difference between the CB and VB is referred to as the bandgap energy (E_g). The positioning of CB and VB, as well as the bandgap, are one of the most critical factors of the semiconductor as it describes light absorption property and the redox reaction ability of the semiconductor, as illustrated in Figure 2.1 below.

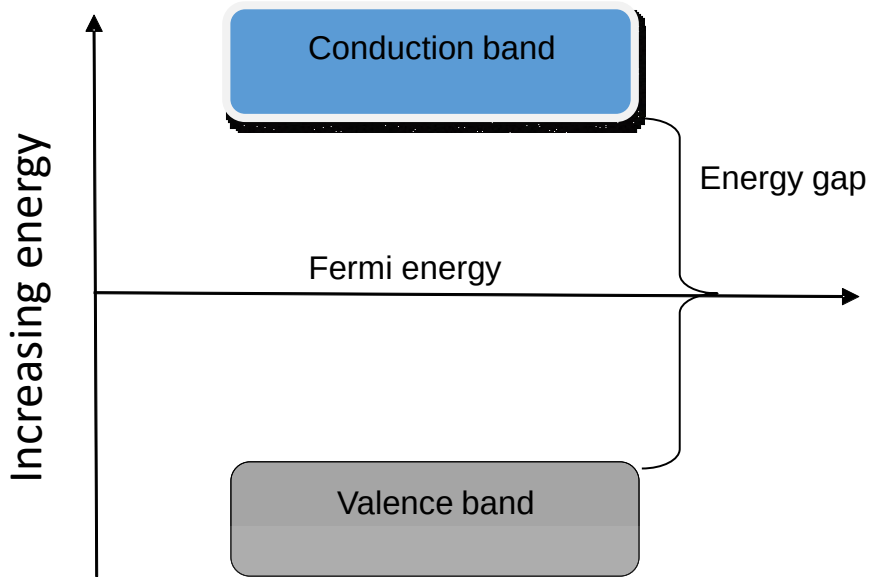

Figure 2.1. Semiconductor illustration of the energy bandgap between the conduction band and valence band.

As the photons are absorbed in the semiconductor (with enough energy to eject electrons), the electrons are promoted to the CB, leaving generated holes in the VB [31]. The formation of free electrons and holes demonstrates that the energy in the semiconductor has been generated.

The major challenge that affect photovoltaic cell efficiency is the loss of electrons through electron-hole recombination. The formation of heterostructures could be more advantageous in providing a direct, quicker and short path for the energized electrons to be distributed to the storage. The longer the electrons spend on the CB, the high chances of the recombination could take place [11].

2.2.2 Two-Dimensional Materials

Graphene, as the early two-dimensional (2D) material, has attracted a lot of attention due to its excellent electron-transport properties and structural features [32]. Though it is useful in the utilization of high-speed electronic device and

photovoltaic cells, it's zero electronic bandgap makes it very difficult to be used in optoelectronic and photovoltaic cells; therefore, graphene needs the incorporation of another material to widen the electronic bandgap and enhance its efficiency. This drawback or limitation led to the continued search for other 2D materials [33, 34].

Several 2D materials have been applied as an alternative substrate to widen up the bandgap of graphene without degrading the properties of the electrons [33, 35]. However, the obtained bandgap is still not big enough for application in electronic devices [36]. Carbon nitride was reported as a promising 2D material to widen up the bandgap of graphene by forming a heterostructure material. A bandgap of about 0.40 eV was reported with an excellent significant electron transfer from graphene to C_2N material [37]. Also, the electronic properties of C_2N and graphene (G) more especially the direct bandgap of C_2N and visible light region are almost well-preserved. These results support the formation of C_2N/G heterostructure to be used as an electronic material for high-performance Field Effect Transistor (FET) devices, water splitting and photovoltaic cells [37].

C_2N has been successfully synthesised via a simple wet bottom-up chemical reaction [38]. The 2D C_2N nanosheet has been theoretically confirmed to be a direct bandgap semiconductor [38]. The theoretical studies have proved that C_2N can be well-tuned by diverging the external electric field, layer number and stacking order for PV application. The unique electronic properties, tunable optical properties, high carrier mobility and chemical stability, offer C_2N a renewed opportunity to be applied in photovoltaic cells [38, 39] and mechanical devices [40], which require a very strong hexagonal network. Figure 2.2 shows the C_2N nanosheet below:

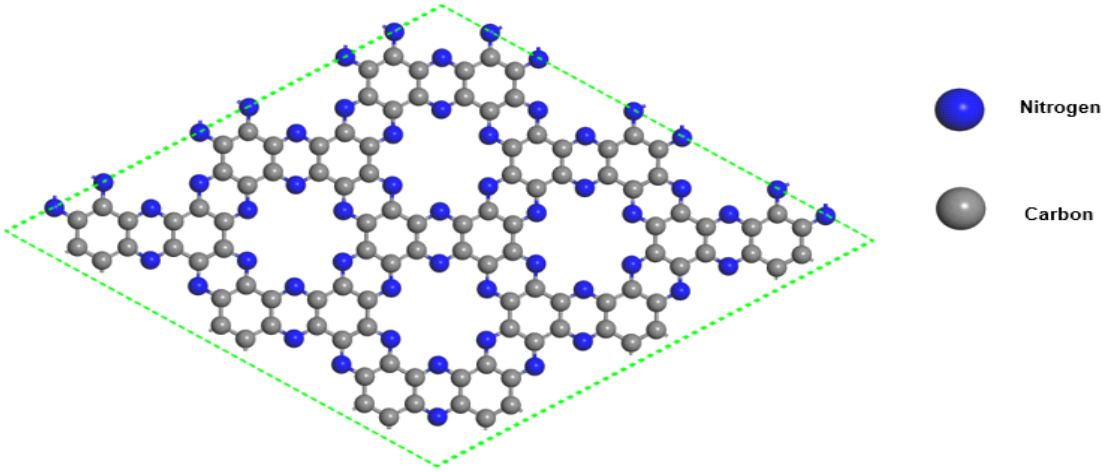

Figure 2.2. Carbon nitride hexagonal structure

2.3 Heterostructure Formation

Recently, efforts have been made to design and construct semiconductor–semiconductor junctions for successful charge separation efficiency, light absorption, and photovoltaic processes. Numerous semiconductors for photovoltaics have a characteristic electronic structure, which can absorb the wider wavelength region and offer different abilities in the separation and transfer of charge carriers. The merging of different semiconductors for photovoltaics use has superb properties that form newly photovoltaic materials with optimum performance. Heterostructures have been grouped into conventional heterojunction, *p*–*n* junction, semiconductor sensitisation and Z–scheme.

2.3.1 Types of Heterostructures Formation

A heterostructure is an interface contact between the two different layers in a photovoltaic with different band structures, which can be tuned in various band alignment. The bandgap, electron affinity and work function are the most important properties of heterostructure materials that define the charge carrier transportation

within the formed heterostructure. Concerning the band alignment of semiconductors, there were three (3) initial types of heterostructures (i.e. straddling, staged and broken gap) for a photovoltaic mechanism have been proposed, as shown in Figure 2.3 and later on another three more were developed, which are explained further on this chapter.

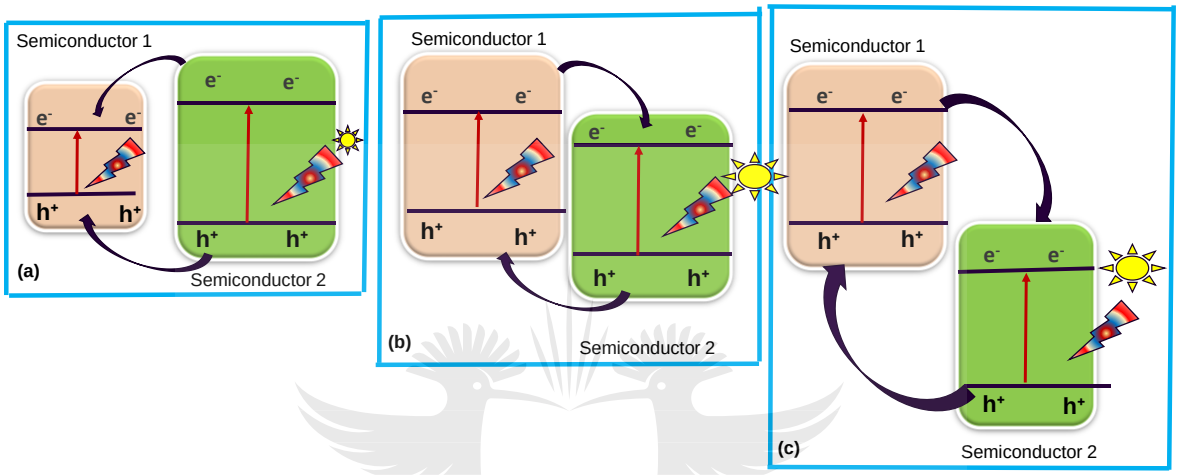

Figure 2.3. Illustration of 3 types of heterostructures for charge separation: (a) Type-I (Straddling gap), (b) Type-II (Staggered gap) and (c) Type-III (Broken gap).

Type–I heterostructure or straddling gap shows the VB and CB of semiconductor 2 as lower and higher than that of semiconductor 1, see in Figure 2.3 (a). Type–I illustrates that the energized electrons and holes cannot be isolated since they have been accumulated on the same semiconductor. Consequently, a semiconductor with a lower redox potential may act as the redox reaction site, thus reducing the ability of redox reaction. With such property, type–I has been used as the luminescent materials for achieving efficient light absorption for solar cells using the material, such as BP/SiC [37]. In the type–II heterostructure (staggered gap) the CB and VB of semiconductor 1 are higher compared to the CB and VB edges of

semiconductor 2, as clearly shown in Figure 2.3 (b). Under visible light radiation, the photogenerated electrons diffuse into semiconductor 2. In contrast, the holes left in the VB moves into semiconductor 1, showing the opposite movement of electrons and holes within the heterostructure. Up to now, several type–II photovoltaic, such as Cs-doped $CH_3NH_3PbI_3$ [41], pentacene/PbSe [42], C_2N/MoS_2 [43], $MoSe_2/MoS_2$ [44, 45] and others [28, 46, 47] have been considered and fabricated with a better photovoltaic performance.

The heterostructures draw an essential role in tuning the photovoltaic properties. For example, porphyrin/ZnO van der Waal heterostructure properties were studied based on the density functional theory (DFT) in conjunction with the projector augmented wave potentials [43]. The electronic band structures of C_2N and MoS_2 are both direct bandgap with a value of 1.66 eV and 1.67 eV, respectively [43]. The formed C_2N/MoS_2 composite showed a reduced direct bandgap of 1.30 eV. It further showed good optical properties that were effectively tuned vertically due to the interaction between d_z^2 orbitals of MoS_2 and P_z orbital of C_2N. The formed C_2N/MoS_2 heterostructure with the reduced bandgap could separate the photoinduced electrons and holes, thus improving the visible-light absorption and promises to be a good semiconductor in photovoltaic cells.

In the type–III heterostructure (broken gap) the CB and VB of semiconductor 1 are higher than those of semiconductor 2, making it an extreme bandgap compared to type-I and type-II heterostructures. The separation and transfer of charge carriers between the two semiconductors cannot occur in the type–III, which makes it unfavourable for photovoltaic activity. Though there is a reported electronic and optoelectronic material, such as MoS_2/C_3N [48] which reveals that type-III

heterostructures also contribute to advancing solar cells, it is not favourable. The larger bandgap of heterostructures makes it more difficult for the band edges to overlap with each other. Therefore, the photogenerated charge carriers between the two semiconductors cannot be transferred in the type-III mechanism, see Figure 2.3 (c).

The poor separation and transfer of charge carriers make type–III unfavourable for application as a photovoltaic material. Amongst these three types of mechanisms, type–II is the most favourable in enhancing the photovoltaic performance with its suitable band alignment for the effective separation of photogenerated charge carriers.

As previously mentioned, there are another three more unconventional types of 2D vdW heterostructures, for band alignments at the interfaces. The schematic photovoltaic mechanisms of these recently reported type-IV to VI 2D vdW heterostructures are presented in Figure 2.4 [49].

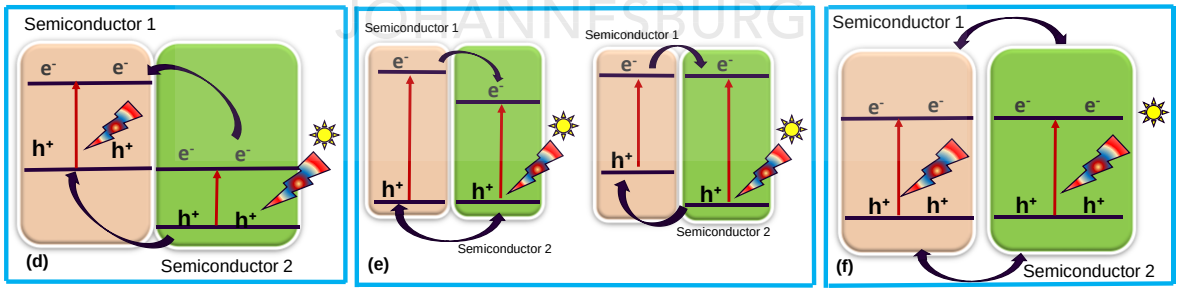

Figure 2.4. Illustration of newly discovered of 2D vdW heterostructures for charge distribution: (a) Type-IV, (b) Type-V and (c) Type-VI.

In recent reports, type IV-VI heterostructures have demonstrated similar physical properties even though they do not have the same band edges shape [50]. Zhang *et al*. have since proved surface properties determined by the surfactants and facet

energy, contain a strong significant effect on the morphology of the heterostructures [51]. Also, the chemical stability of the composition in the type-VI heterostructure is carefully considered [52]. Furthermore, they show the advantages of alloy composition combined with core/shell heterostructure [53].

Type-IV and type-V band alignments have been reported that the interactions between various band layers could bring the hybridization of the p and/or s orbitals, thereby leading to the division of band edges of multilayers of type-IV and type-V semiconductors [54, 55]. The explained property has been presented in the vdW heterostructures constructed in Figure 2.4 (b) and (c).

Based on first-principles calculations, type-IV band alignment allows electrons from semiconductor 1 to semiconductor 2 and holes from semiconductor 1 to semiconductor 2. In type-IV, after the irradiation of visible light on the surface of the heterostructure, the electron-holes pairs are separated with advantages of electrons and holes transferring to CB and VB, respectively. The mechanism of type-IV shows that there is possible recombination of electron-hole pairs from the VB and CB of the respective semiconductors since they are slightly aligned close to each other.

In type-V band alignment, there are two types of formations. For the first formation, the VB of the two semiconductors is aligned together with the possible movement from semiconductor 1 to semiconductor 2. Therefore remaining holes in the VB of the two semiconductors. The dislodging of electrons in both semiconductors requires an equal amount of energy. The CB of the two semiconductors is not aligned together, thus allowing electrons from semiconductor 1 to semiconductor 2. In the second formation, the CB on the two semiconductors is aligned with the relaxed movement of photogenerated electrons from semiconductor 1 and

semiconductor 2 and vice versa. The VB of semiconductor 2 is lower to that of semiconductor 1, with the possible movement of holes from VB of semiconductor 2 to semiconductor 1.

In type-VI band alignment, there is a common form of alignment in CB and VB semiconductors. The CB of semiconductor 1 is aligned together with the CB of semiconductor 2. The VB of semiconductor 1 is aligned to the VB of semiconductor 2 [56]. The type-VI formation can be prompted by coupling well stable interlayers of the 2D heterostructure. Since both CBM and VBM are delocalized in both alignment, the photogenerated electron-hole pairs can be separated and transferred spontaneously.

2.3.2 Absorption of Visible Light and Electronic Band Structures

The absorption of visible light within the intensity region of the visible spectrum plays a crucial part in photovoltaic performance [57]. The reduction of a bandgap can efficiently improve the transfer charge carrier, that is having a small bandgap distance to reach the interface of another semiconductor. Visible light absorption requires a proper CB and VB edge positioning for better absorption of light intensity. Also, visible light has a positive impact on the charge carriers generation.

Electronic band structures influence light absorption, charge separation and charge carrier for chemical reactions [57]. This affects the performance of semiconductor under visible light. The band structure can influence the reactions involved in the photovoltaic process and control the wavelength region of absorbed light within the semiconductor [58].

2.4 Photovoltaic Characteristics

In PVs, three classical parameters are highly crucial; namely, open-circuit voltage (V_{oc}), short-circuit current (J_{sc}) and the maximum fill factor (FF). The fill factor provides the maximum power to the photovoltaic cells. The FF parameter describes how close the cell behaves to the step-function ideal diode. This can lead to a better design technique and improvement of the competitiveness of semiconductors with thin-film technologies. J_{sc} has been improved through low bandgap to harvest more sunlight while V_{oc} has been increased by lowering donor electrons and reducing the recombination between the acceptor and donor. The calculation of power conversion efficiency (PCE) is achieved by increasing FF, J_{sc} and V_{oc} [59].

2.5 Hybrid Carbon Nitride-Semiconductors

Efficient carrier separation and appropriate band structure are critical to the development of better photovoltaic devices. The C_2N/GaTe heterostructure found to be an indirect bandgap material of Eg = 1.39 eV from C_2N monolayer (2.42 eV) and GaTe monolayer (2.04 eV), proves that the band gap has been reduced and this suggests that the C_2N/GaTe heterostructure can effectively reduce the bandgap and enhances the transfer of photogenerated electrons [28]. Also, the CB was contributed by C_2N, whereas the VB was contributed by GaTe monolayer, indicating the formation of the type-II heterostructure as can be seen in Figure 2.3 (b). Therefore, promoting an efficient photogenerated separation of charge carrier is well reliable with the partial charge density of VB and CB of C_2N/GaTe heterostructure.

2.6 Hybrid PV Cells Based on Polythiophenes

These particular devices are usually hybrid solar cells and their content are established on the mixtures of poly(3-hexylthiophene-2,5-diyl) (P3HT) with cadmium selenide (CdSe), gallium arsenide (GaAs), titanium dioxide (TiO_2) and zinc oxide (ZnO) [60]. An organic-photovoltaic cell (OPV) based on poly(3-methyl-thiophene) was the first one to be reported having a power conversion efficiency of 0.007% and an incident light intensity of 1 mW cm^{-2} [61]. The power conversion efficiency was very low. This has made the researcher to investigate how to improve its efficiency. Several polythiophenes have been reported with the highest efficiency of 5.2 % for P3HT [62].

2.7 References

[1] A. Shah, P. Torres, R. Tscharner, N. Wyrsch and H. Keppner. Photovoltaic technology: the case for thin-film solar cells. *Science* **285** (1999) 692-698.

[2] A. Mujica, A. Rubio, A. Munoz and R. Needs. High-pressure phases of group-IV, III–V, and II–VI compounds. *Rev. Mod. Phys.* **75** (2003) 863-912.

[3] S. Rehman, M. A. Bader and S. A. Al-Moallem. Cost of solar energy generated using PV panels. *Renewable Sustainable Energy Rev.* **11** (2007) 1843-1857.

[4] T. Bruton. General trends about photovoltaics based on crystalline silicon. *Sol. Energy Mater. Sol. Cells* **72** (2002) 3-10.

[5] P. Singh and S. Gupta. Photovoltaic surface in plug-in electric vehicle (Pev) using nanotechnology. *J. Sci.* **5** (2019) 33-38.

[6] M. Hamadanian, J. Safaei-Ghomi, M. Hosseinpour, R. Masoomi and V. Jabbari. Uses of new natural dye photosensitizers in fabrication of high potential dye-sensitized solar cells (DSSCs). *Mater. Sci. Semicond. Process.* **27** (2014) 733-739.

[7] Z.-S. Huang, T. Hua, J. Tian, L. Wang, H. Meier and D. Cao. Dithienopyrrolobenzotriazole-based organic dyes with high molar extinction coefficient for efficient dye-sensitized solar cells. *Dyes Pigm.* **125** (2016) 229-240.

[8] S. Ito, T. N. Murakami, P. Comte, P. Liska, C. Grätzel, M. K. Nazeeruddin and M. Grätzel. Fabrication of thin film dye sensitized solar cells with solar to electric power conversion efficiency over 10%. *Thin solid films* **516** (2008) 4613-4619.

[9] G. Smestad. Testing of dye sensitized TiO_2 solar cells II: Theoretical voltage output and photoluminescence efficiencies. *Sol. Energy Mater. Sol. Cells* **32** (1994) 273-288.

[10] P. Wang, S. M. Zakeeruddin, P. Comte, R. Charvet, R. Humphry-Baker and M. Grätzel. Enhance the performance of dye-sensitized solar cells by co-grafting amphiphilic sensitizer and hexadecylmalonic acid on TiO_2 nanocrystals. *J. Phys. Chem. B* **107** (2003) 14336-14341.

[11] A. A. Husain, W. Z. W. Hasan, S. Shafie, M. N. Hamidon and S. S. Pandey. A review of transparent solar photovoltaic technologies. *Renewable Sustainable Energy Rev.* **94** (2018) 779-791.

[12] K. Chopra, P. Paulson and V. Dutta. Thin-film solar cells: an overview. *Prog. Photovolt.* **12** (2004) 69-92.

[13] F. E. Ala'a, J.-P. Sun, I. G. Hill and G. C. Welch. Recent advances of non-fullerene, small molecular acceptors for solution processed bulk heterojunction solar cells. *J. Mater. Chem. A* **2** (2014) 1201-1213.

[14] S. Hore, C. Vetter, R. Kern, H. Smit and A. Hinsch. Influence of scattering layers on efficiency of dye-sensitized solar cells. *Sol. Energy Mater. Sol. Cells* **90** (2006) 1176-1188.

[15] R. R. Lunt and V. Bulovic. Transparent, near-infrared organic photovoltaic solar cells for window and energy-scavenging applications. *Appl. Phys. Lett.* **98** (2011) 61-66.

[16] R. Betancur, P. Romero-Gomez, A. Martinez-Otero, X. Elias, M. Maymó and J. Martorell. Transparent polymer solar cells employing a layered light-trapping architecture. *Nat. Photonics* **7** (2013) 995-1000.

[17] P. You, G. Tang and F. Yan. Two-dimensional materials in perovskite solar cells. *Mater. Today* **11** (2019) 128-158.

[18] K.-S. Chen, J.-F. Salinas, H.-L. Yip, L. Huo, J. Hou and A. K.-Y. Jen. Semi-transparent polymer solar cells with 6% PCE, 25% average visible transmittance and a color rendering index close to 100 for power generating window applications. *Energy. Environ. Sci.* **5** (2012) 9551-9557.

[19] Q. Dong, Y. Zhou, J. Pei, Z. Liu, Y. Li, S. Yao, J. Zhang and W. Tian. All-spin-coating vacuum-free processed semi-transparent inverted polymer solar cells with PEDOT: PSS anode and PAH-D interfacial layer. *Org. Electron.* **11** (2010) 1327-1331.

[20] Y. Zhao, G. A. Meek, B. G. Levine and R. R. Lunt. Near-infrared harvesting transparent luminescent solar concentrators. *Adv. Opt. Mater.* **2** (2014) 606-611.

[21] C. Roldán-Carmona, O. Malinkiewicz, R. Betancur, G. Longo, C. Momblona, F. Jaramillo, L. Camacho and H. J. Bolink. High efficiency single-junction semitransparent perovskite solar cells. *Energy Environ. Sci.* **7** (2014) 2968-2973.

[22] A. Mei, X. Li, L. Liu, Z. Ku, T. Liu, Y. Rong, M. Xu, M. Hu, J. Chen and Y. Yang. A hole-conductor–free, fully printable mesoscopic perovskite solar cell with high stability. *Science* **345** (2014) 295-298.

[23] A. Fahrenbruch and R. Bube. Fundamentals of solar cells: photovoltaic solar energy conversion. *Elsevier*, (2012)

[24] P. D. Maycock. Photovoltaic technology, performance, manufacturing cost and markets, in Solar 99 conference: Proceedings of ASES annual conference--Proceedings of 24th national passive solar conference, 1999.

[25] E. Assadourian, T. Prugh and L. Starke. State of the World 2013: Is sustainability still possible? *Springer*, (2013)

[26] J. M. Burst, J. N. Duenow, D. S. Albin, E. Colegrove, M. O. Reese, J. A. Aguiar, C.-S. Jiang, M. Patel, M. M. Al-Jassim and D. Kuciauskas. CdTe solar cells with open-circuit voltage breaking the 1 V barrier. *Nat. Energy* **1** (2016) 1-8.

[27] W. Shockley and H. J. Queisser. Detailed balance limit of efficiency of p-n junction solar cells. *J. Appl. Phys.* **32** (1961) 510-519.

[28] Y. Bai, Q. Zhang, N. Xu, K. Deng and E. Kan. Efficient carrier separation and band structure tuning of two-dimensional C_2N/GaTe van der Waals heterostructure. *J. Phys. Chem. C* **122** (2018) 15892-15902.

[29] D. P. Hagberg, T. Marinado, K. M. Karlsson, K. Nonomura, P. Qin, G. Boschloo, T. Brinck, A. Hagfeldt and L. Sun. Tuning the HOMO and LUMO energy levels of organic chromophores for dye sensitized solar cells. *J. Org. Chem.* **72** (2007) 9550-9556.

[30] H. Spanggaard and F. C. Krebs. A brief history of the development of organic and polymeric photovoltaics. *Sol. Energy Mater. Sol. Cells* **83** (2004) 125-146.

[31] F. Opoku, K. K. Govender, C. G. C. E. van Sittert and P. P. Govender. Recent progress in the development of semiconductor-based photocatalyst materials for applications in photocatalytic water splitting and degradation of pollutants. *Adv. Sustainable Syst.* **1** (2017) 1700006-1700030.

[32] H. Hosokawa, R. Tamaki, T. Sawada, A. Okonogi, H. Sato, Y. Ogomi, S. Hayase, Y. Okada and T. Yano. Solution-processed intermediate-band solar

cells with lead sulfide quantum dots and lead halide perovskites. *Nat. Commun.* **10** (2019) 1-8.

[33] F. Schwierz. Nanoelectronics: Flat transistors get off the ground. *Nat. Nanotechnol.* **6** (2011) 135-136.

[34] A. C. Neto, F. Guinea, N. M. Peres, K. S. Novoselov and A. K. Geim. The electronic properties of graphene. *Rev. Mod. Phys.* **81** (2009) 109-164.

[35] N. Kharche and S. K. Nayak. Quasiparticle band gap engineering of graphene and graphone on hexagonal boron nitride substrate. *Nano Lett.* **11** (2011) 5274-5278.

[36] R. Decker, Y. Wang, V. W. Brar, W. Regan, H.-Z. Tsai, Q. Wu, W. Gannett, A. Zettl and M. F. Crommie. Local electronic properties of graphene on a BN substrate via scanning tunneling microscopy. *Nano Lett.* **11** (2011) 2291-2295.

[37] D. Wang, D. Han, L. Liu and L. Niu. Structure and electronic properties of C_2N/graphene predicted by first-principles calculations. *RSC Adv.* **6** (2016) 28484-28488.

[38] J. Mahmood, E. K. Lee, M. Jung, D. Shin, I.-Y. Jeon, S.-M. Jung, H.-J. Choi, J.-M. Seo, S.-Y. Bae and S.-D. Sohn. Nitrogenated holey two-dimensional structures. *Nat. Commun.* **6** (2015) 1-7.

[39] S. Z. Butler, S. M. Hollen, L. Cao, Y. Cui, J. A. Gupta, H. R. Gutiérrez, T. F. Heinz, S. S. Hong, J. Huang and A. F. Ismach. Progress, challenges, and opportunities in two-dimensional materials beyond graphene. *ACS Nano* **7** (2013) 2898-2926.

[40] S. Savagatrup, A. D. Printz, T. F. O'Connor, A. V. Zaretski, D. Rodriquez, E. J. Sawyer, K. M. Rajan, R. I. Acosta, S. E. Root and D. J. Lipomi. Mechanical

degradation and stability of organic solar cells: molecular and microstructural determinants. *Energy Environ. Sci.* **8** (2015) 55-80.

[41] A. Taya, P. Rani, J. Thakur and M. K. Kashyap. First principles study of structural, electronic and optical properties of Cs-doped $CH_3NH_3PbI_3$ for photovoltaic applications. *Vacuum* **160** (2019) 440-444.

[42] P. Roy and T. P. Nguyen. Ab initio calculation of pentacene–PbSe hybrid interface for photovoltaic applications. *Phys. Chem. Chem. Phys.* **18** (2016) 18209-18218.

[43] Z. Guan, C.-S. Lian, S. Hu, S. Ni, J. Li and W. Duan. Tunable structural, electronic, and optical properties of layered two-dimensional C_2N and MoS_2 van der waals heterostructure as photovoltaic material. *J. Phys. Chem. C* **121** (2017) 3654-3660.

[44] H. Tian, M. L. Chin, S. Najmaei, Q. Guo, F. Xia, H. Wang and M. Dubey. Optoelectronic devices based on two-dimensional transition metal dichalcogenides. *Nano Res.* **9** (2016) 1543-1560.

[45] R. Long and O. V. Prezhdo. Quantum coherence facilitates efficient charge separation at a MoS_2/$MoSe_2$ van der Waals junction. *Nano lett.* **16** (2016) 1996-2003.

[46] P. J. Jeon, J. S. Kim, J. Y. Lim, Y. Cho, A. Pezeshki, H. S. Lee, S. Yu, S.-W. Min and S. Im. Low power consumption complementary inverters with n-MoS_2 and p-WSe_2 dichalcogenide nanosheets on glass for logic and light-emitting diode circuits. *ACS Appl. Mater. Interfaces* **7** (2015) 22333-22340.

[47] Y. Yu, S. Hu, L. Su, L. Huang, Y. Liu, Z. Jin, A. A. Purezky, D. B. Geohegan, K. W. Kim and Y. Zhang. Equally efficient interlayer exciton relaxation and

improved absorption in epitaxial and nonepitaxial MoS_2/WS_2 heterostructures. *Nano lett.* **15** (2015) 486-491.

[48] Y. Yang and Z. Wang. A two-dimensional MoS_2/C_3N broken-gap heterostructure, a first principles study. *RSC Adv.* **9** (2019) 19837-19843.

[49] Y. Si, H.-Y. Wu, J.-C. Lian, W.-Q. Huang, W.-Y. Hu and G.-F. Huang. A design rule for two-dimensional van der Waals heterostructures with unconventional band alignments. *Phys. Chem. Chem. Phys.* **22** (2020) 3037-3047.

[50] J. Tian, Z. Zhao, A. Kumar, R. I. Boughton and H. Liu. Recent progress in design, synthesis, and applications of one-dimensional TiO_2 nanostructured surface heterostructures: a review. *Chem. Soc. Rev.* **43** (2014) 6920-6937.

[51] Z. Zhang, Q. Qian, B. Li and K. J. Chen. Interface engineering of monolayer MoS_2/GaN hybrid heterostructure: modified band alignment for photocatalytic water splitting application by nitridation treatment. *ACS Appl. Mater. Interfaces* **10** (2018) 17419-17426.

[52] L. J. Lauhon, M. S. Gudiksen, D. Wang and C. M. Lieber. Epitaxial core–shell and core–multishell nanowire heterostructures. *Nature* **420** (2002) 57-61.

[53] F. M. Pope, G. R. Martin, J. R. Lichtenstein, R. Penttinen, B. Gerson, D. W. Rowe and V. A. McKusick. Patients with Ehlers-Danlos syndrome type IV lack type III collagen. *Proc. Natl. Acad. Sci.* **72** (1975) 1314-1316.

[54] C.-Y. Yeh, S.-H. Wei and A. Zunger. Relationships between the band gaps of the zinc-blende and wurtzite modifications of semiconductors. *Phys. Rev. B* **50** (1994) 2715-2719.

[55] R. Chandiramouli and S. Sriram. A DFT study on ternary compounds of GaAlAs and InAlAs nanoclusters. *Mater. Sci. Semicond. Process.* **27** (2014) 800-809.

[56] A. Maharjan, K. Pemasiri, P. Kumar, A. Wade, L. Smith, H. Jackson, J. Yarrison-Rice, A. Kogan, S. Paiman and Q. Gao. Room temperature photocurrent spectroscopy of single zincblende and wurtzite InP nanowires. *Appl. Phys. Lett.* **94** (2009) 193115-193119.

[57] Z. Li, W. Luo, M. Zhang, J. Feng and Z. Zou. Photoelectrochemical cells for solar hydrogen production: current state of promising photoelectrodes, methods to improve their properties, and outlook. *Energy Environ. Sci.* **6** (2013) 347-370.

[58] M. S. Benghanem and S. N. Alamri. Modeling of photovoltaic module and experimental determination of serial resistance. *J. Taibah. Univ. Sci.* **2** (2009) 94-105.

[59] A. Kamble, K. Mokurala, A. Gupta, S. Mallick and P. Bhargava. Synthesis of Cu_2NiSnS_4 nanoparticles by hot injection method for photovoltaic applications. *Mater. Lett.* **137** (2014) 440-443.

[60] Y. Wang, Q. Wang, X. Zhan, F. Wang, M. Safdar and J. He. Visible light driven type II heterostructures and their enhanced photocatalysis properties: a review. *Nanoscale* **5** (2013) 8326-8339.

[61] K. M. Coakley and M. D. McGehee. Conjugated polymer photovoltaic cells. *Chem. Mater.* **16** (2004) 4533-4542.

[62] S. Glenis, G. Horowitz, G. Tourillon and F. Garnier. Electrochemically grown polythiophene and poly (3-methylthiophene) organic photovoltaic cells. *Thin solid films* **111** (1984) 93-103.

CHAPTER 3:

COMPUTATIONAL FUNDAMENTALS AND METHODOLOGY

The theoretical methods used in this research are presented in this section. All our calculations were based on first-principles.

3.1 Computational Methods

3.1.1 Quantum Physics (Quantum Mechanics)

Quantum physics (Quantum mechanics) provides clear theory on the modern basis on how an electron behaves and the different energies on the atomic and sub-atomic levels of matter. It further describes any properties of the individual atoms or molecules [1].

Well, known scientists (Heisenberg and Schrödinger) developed an equation of quantum mechanics to describe the quantum mechanical system's wave function or state function. A linear equation of Schrödinger is shown in equation 3.1 [2]:

$$\hat{H}\Psi = E\Psi \tag{3.1}$$

where $\hat{H}$ is the Hamiltonian operator, Ψ is the wave function of an electron and nuclear position, E is the energy of an electron, called eigenvalue and Ψ is the Eigen function. The presented equation is referred to as the Eigen equation.

For the electrons interchanged, the wave function should be continuous, anti-symmetric, normalized and single-value to solve the physical equation of Schrödinger. The Hamiltonian ($\hat{H}$) operator is defined further in equation 3.2.

$$\hat{H} = -\sum_{i}^{particles} \frac{\nabla_I^2}{2m_i} + \sum_{i<j}^{particles} \sum_{i}^{n} \frac{q_i q_j}{r_{ij}} \quad (3.2)$$

$$\nabla_I^2 = \frac{\partial^2}{\partial x_i^2} + \frac{\partial^2}{\partial y_i^2} + \frac{\partial^2}{\partial z_i^2} \quad (3.3)$$

where q_i represents the charge of the particle, i and m_i represent the mass of the particle, r_{ij} represents the distance between the particles and ∇_I^2 represents the particle (equation 3.3).

3.1.2 Semi-Empirical (SE) Methods

The semi-empirical method is estimated by collecting spectroscopic data and / or physical properties, such as electron affinity using wave functions. The collected data is treated using series of rules to set certain integrals to equal to zero. Only minimal basis sets are engaged in semi-empirical calculations, while the two electrons and core electron integrals are parameterized from the experimental data [3]. Compared to ab initio methods, semi-empirical is faster but provides inaccurate results due to the applied parameters. Semi-empirical methods can also be applied in computing of molecular properties, such as electronic spectra and ionization potential [4]. Some of the used SE methods are Austin Model 1, Parameterization Method 2 and Complete Neglect of Difference Overlap.

3.1.3 The *Ab Initio* Method

The *ab initio* method, also referred to as the electronic structure method, is directly used in theoretical calculations where there are no experimental data to rely on [5]. This method relies on resolving the electronic state within the system and allows the various properties of the system to be calculated. The laws of quantum mechanics are applied to the *ab initio* method to acquire the properties of chemical species [5, 6]. The electrons likelihood density is expressed as wave function squared (ψ^2). *Ab*

initio is usually expensive and takes a large amount of disk space, memory and central processing unit (CPU). Hartree-Fock (HF) theory is the frequently used *ab initio* method.

3.2 Density Functional Theory (DFT)

The quantum mechanical treatment of materials requires the calculations of the many-nuclei or many-electron wave function of a system. However, the moderate expansive mass of the cores implies that for the endless larger part of the reenactments their behaviour is decoupled from the electrons and may be treated as classical point-like particles [7]. Concerning the cores, the mass of electrons implies that a full quantum mechanical treatment is required to get to their behaviour.

In any case, density functional theory (DFT) permits us to address computational difficulty by centering on the electron density rather than the many-body wave function. The basic rule of DFT is that the full vitality of the framework could be a special function of the electron density; subsequently, it is superfluous to compute the total many-body wave function of the system. However, the exact useful reliance of the energy on the density is not known. The DFT computational codes are used in practice to explore the electronic properties, structural defects and magnetism of materials at the atomic level [8].

Kohn and Sham density functional theory calculations are based on the Born Oppenheimer approximation on the orbitals [9]. The Kohn and Sham equations comprise of N-single particle (three-dimensional) Schrödinger like equations with adjusted successful potential. They are much simpler to illuminate than the initial (3N-dimensional) many-body issue [10]. DFT offers a balance between accuracy and computational efficiency well suited to most materials applications [11]. DFT

Simulation may be performed routinely on systems of hundreds of molecules, with calculations for thousands of particles being requested.

3.3 Background on Density Functional Theory

3.3.1 Thomas-Fermi Theorem

The first discovery of the direct correlation between the wave function of the many-electron molecule and electron density of the molecule was done by Thomas and Fermi [12]. The expression (equation 3.4) is used to determine the electron`s kinetic energy, where the electron-electron interaction and electron-nucleus are treated classically.

$$E_T = \frac{2}{10}\frac{\hbar(3\pi^2)^{2/3}}{m}\int[n(\vec{r})^{\frac{5}{3}}\,d^3r + \int V_{ext}(\vec{r})d^3 + \int n(r)V_H(\vec{r})d^3\,r \qquad (3.4)$$

Thomas-Fermi (TF) theory describes the functional form of the kinetic energy of the non-interacting system, where the density is a function of the position *n(r)* and one can assume that the same functional form and the Fermi momentum becomes position-dependent [12]. The quantum theory is used to determine electrons kinetic energy; electron-electron and electron-nucleus interactions are treated. The electrons kinetic energy is shown in equation 3.5.

$$T[n] = C_F \int n^{\frac{5}{3}}(r)dr, \qquad (3.5)$$

where $C_F = \frac{3}{10}(2\pi^2)^{\frac{2}{3}}$ = 2.871. The total energy of the electron density has obtained by the sum of interactions between the electron-nucleus and electron-electron equation 3.6 [14].

$$E[n] = C_F \int n^{\frac{5}{3}}(r)dr - Z\int \frac{n(r)}{r}dr + \frac{1}{2}\iint \frac{n(r_1)n(r_2)}{[r_1-r_2]}dr_1dr_2 \qquad (3.6)$$

3.3.2 Hohenberg-Kohn Theorem

Hohenberg together with Kohn was the first to determine the DFT calculations basis set. They both came up with a proposal that the ground-state of any interacting many-electron system with a given fixed inter electron interaction is a unique function of the electron density and all the properties of the ground electrons can be calculated. Their model depended on electron density with an external potential and the principle of variation, which is used to determine the density of an electron at its ground state [15]. Hohenberg and Kohn's model assumes that knowing the electron density and universal functional will help determine the ground state energy density [15]. However, this enabled the description of the ground state energy *E* as a function of the ground state, as shown below:

$$E\left[\Psi[n_0]\right] = \langle \psi[n_0] \vee T + V \vee \psi[n_0] \rangle \tag{3.7}$$

Equation 3.7 indicates the sum of the kinetic energy and the repulsion of electron-electron operation with ground-state wave function.

3.3.3 Kohn-Sham Model

In the early 1960s, Kohn and Sham further developed DFT after realizing that the theory of Thomas-Fermi was poor in giving more explanation on the minimum energy of the electron [13]. Kohn and Sham [16] showed that looking for the right electron density could be expressed in several ways that included solving equations with each equation only involving a single electron in the calculation. The equation 3.8 was formed as:

$$\left[\frac{h^2}{2m}\nabla^2 + V(r) + V_H(r) + V_{XC}(r)\right]\psi_i(r) = \varepsilon_i\psi_i(r) \tag{3.8}$$

The equations of Kohn-Sham are for single-electron wave function that relies on three spatial variables only, $\psi_i(r)$.

Hartree-Fock Method (HF)

The theory of Hartree-Fock is one of the used method in the *ab initio*. The HF method is used to approximate the determination of the wave function and energy of a quantum many-body system in a stationary state. The HF method formulates the core of the molecular orbital (MO) theory, which is used to describe the movement of each electron. One of the advantages of using the HF method is to separate the many-electron Schrödinger equation into the individual one-electron equation state. In the HF method, the electron-electron interaction is not considered; only the average impact of repulsion of the electron is considered.

Derivation of Hartree-Fock Equations

To find the best molecular orbitals, firstly those that minimise $\bar{E}$, those are MOs wave function for which minimise $\bar{E}$ is stationary to its small variations $\delta\Phi$. The variation of MOs is done in a varied way that it does not destroy their orthonormality since it has been derived in the equation of minimising $\bar{E}$ as generalised to the 2n-electron, closed-shell case and adding in another contribution electron:

$$\bar{E} = \langle \psi_{2n} | \hat{H} | \psi_{2n} \rangle = 2 \sum_{i=1}^{n} H_{ii} + \sum_{i=1}^{n} \sum_{j=1} n \qquad (3.9)$$

The above equation is desired to express the $\bar{E}$ in terms of the integrals over the MOs Φ_i for a single determination, closed-shell wave function.

This shows that correct variation of δΦ at the minimum $\bar{E}$, both MO and $\bar{E}$ overlap integrals $s_{ij} = \langle \Phi_i \vee \Phi_j \rangle$ should remain constant. s_{ij} must be equal to unity when *i=j* or otherwise zero. If s_{ij} and $\bar{E}$ remains constant; the linear combination is constant.

This provides the equation with the minimum $\bar{E}$ for the restricted type of $\delta\Phi$ as follows:

$$C_0\bar{E} + \sum_i \sum_j c_i s_j = \text{constant} \quad (3.10)$$

The equation holds any set of coefficient *c* as long as δΦ is restricted adequately in nature. Conversely, it is possible to illustrate that a particular set of coefficients in equation 3.5 is at the minimum $\bar{E}$ for any small variations δΦ. This specific coefficient is referred to as Lagrangian multipliers. They are of undetermined value, but their values will be known when the problem is solved.

3.4 Exchange-Correlation Functional

The exchange-correlation functional energy must be known to employ the Kohn-Sham theorem. What challenges the density functional theory is that the exchange-correlation functional in the respective equations is unknown [17]. The exchange-correlation is calculated by assuming an approximate type of reliance on the exchange-correlation energy to assess the functional derivative and electron density. A collection of functions has been developed, such as local and non-local functional, to improve accuracy [17]. Local density approximation (LDA) functional depends on the electron density, while non-local depend on both the gradient and electron density. For such reason, LDA is the most widely used approximation and is defined by:

$$E_{XC}^{LDA} = \int d^3 \, re_{XC}^{hom}(n_o)_{n_o \to n(r)} \quad (3.11)$$

where $re_{XC}^{hom}(n_o)_{n_o \to n(r)}$ represent the exchange-correlation energy of each particle of the homogenous electron and replacing it with a constant density of n_0 by local density $n(r)$ of the inhomogeneous method.

The LDA is efficient for geometrical quantities, such as bond length, electron density, energy differences (e.g., ionization potential) and vibrational frequencies. The improvements are made based on the results obtained by Hartree-Fock approximation. The LDA functional overestimates the ground state energies compared with Hartree-Fock approximation and experimental data [18]. Also, LDA typically performs poorly in some quantities, such as atomization energy and bond dissociation energy. The Jabob`s Ladder shows various sets of exchange-correlation approximations been made and the function that was proposed by Perdew, as shown in Figure 3.1 below:

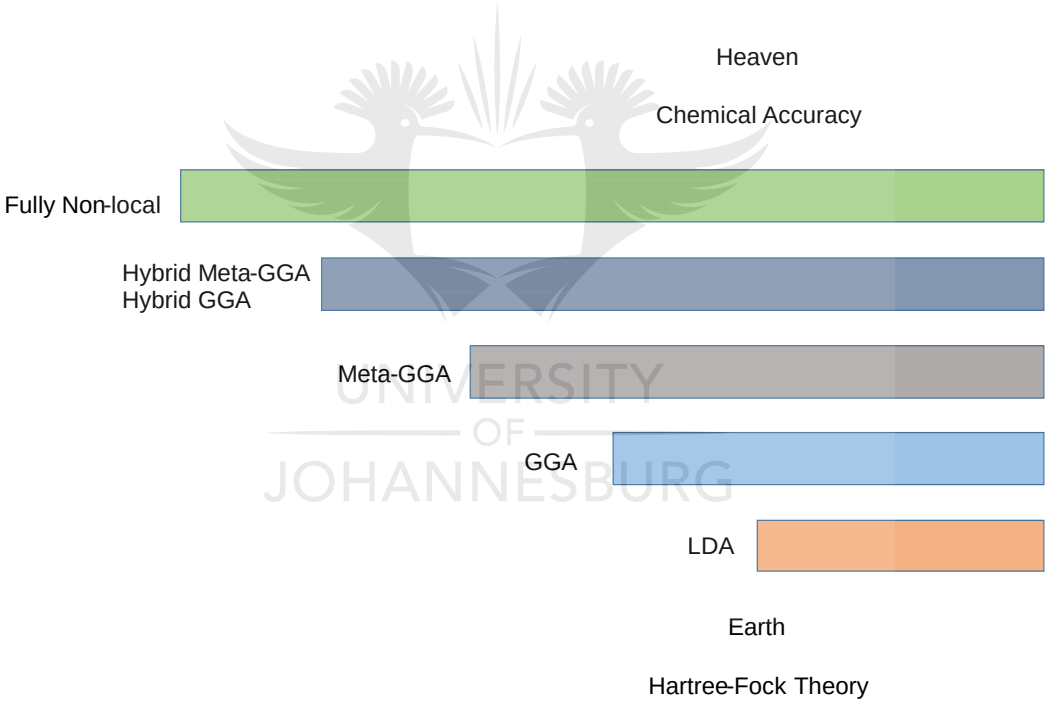

Figure 3.1. Diagram of exchange-correlations functional accuracy (Jacobs Ladder).

Functionals can be classified as empirical and non-empirical regarding their intricacy on the levels of ladder scale, i.e. the Hartree approximations for defining the

exchange-correlations. The functional form for the exchange-correlation energies gives the reliability of using different DFT approaches.

(a) Generalized Gradient Approximation

The generalized gradient approximation (GGA) is an improvement functional from LDA to give good results in the low-order gradient in LDA; thus, introducing gradient density $(\mathrm{n}, \nabla \mathrm{n})$ was useful [19]. The gradient density $(\mathrm{n}, \nabla \mathrm{n})|$ is introduced in the generalized gradient approximation as an independent variable. The gradient density incorporation is non-local in the exchange-correlation function, which is expressed in terms of the densities and local gradients as follows:

$$\mathrm{E}_{\mathrm{XC}}^{\mathrm{GGA}} = \int \mathrm{d}^3 \mathrm{r} \mathrm{e}_{\mathrm{XC}}^{\mathrm{GGA}}(\mathrm{n}, \nabla \mathrm{n}) \tag{3.12}$$

The introduced functional $\mathrm{e}_{\mathrm{XC}}^{\mathrm{GGA}}(\mathrm{n}, \nabla \mathrm{n})$ represents a factor for improving the exchange and multiple forms have been proposed. The proposed functionals use the effective potential of asymptotic behaviour, general scaling properties, sum rules, and many others [20]. The commonly used GGA functionals were derived by Perdew, Burke and Ernzerhof and Perdew and Wang [21].

(b) Heyd-Scuseria-Ernzerhof (HSE) Functional

The exchange-correlation functional is calculated approximately within GGA and LDA. One of the challenges in evaluating the Hartree-Fock functional exchange is the dissolution of the exchange interaction distance. This can be done by integrating the Kohn-Sham correlation energy and HF exchange energy, where the description of exchange-correlation functional can be well explained [22]. The hybrid functional was recommend and used by Heyd, where the exchange interactions in both short and long ranges are apart [23]. The short-range part is overcome by the mixture of

DFT and HF exchange, while the long-range part is resolved by classifying only the corresponding part of the separating DFT. Comparing the HSE with PBE0 functional, the HSE gives an improved result for molecular properties and show enhancement over PBE0 functional. The PBE0 functional together with Perdew-Burke-Ernzerhof (PBE) and Hartree-Fock exchange-correlation energy is expressed as:

$$E_{XC}^{PBE0} = \frac{1}{4}E_X^{HF} + \frac{3}{4}E_X^{PBE} + E_C^{PBE} \quad (3.13)$$

where E_X^{PBE}, E_X^{HF} and E_C^{PBE} represent PBE exchange functional, Hartree-Fock exchange and PBE exchange-correlation functional. Furthermore, the HSE for exchange-correlation functional is expressed as:

$$E_{XC}^{HSE} = \alpha E_x^{SR}(\mu) + (1\text{-}\alpha)E_x^{PBE,SR}(\mu) + E_x^{PBE,LR}(\mu) + E_x^{PBE}(\mu) \quad (3.14)$$

where $E_x^{PBE,SR}$ is the short-range part and $E_x^{PBE,LR}$ is the long-range part for PBE exchange-correlation energies. The short-range for Hartree-Fock energy is E_x^{SR} and alpha (α) is the mixing coefficiency. The μ signifies the screening parameter to evaluate the short-range and long-range interaction separately.

3.5 Simulation Software

3.5.1 Materials Studio 2019

Materials Studio is a state-of-art simulation package [24, 25], which allows researchers in the field of material science [26] and chemistry [27] to predict and understand thoroughly molecular structure and materials using computers. Calculations performed with Materials Studio software offer valid, comprehensive and efficient results by quantum mechanical equations with DFT methods [28].

Materials Studio software can also perform calculations using semi-empirical methods, hybrid quantum mechanics and/or molecular mechanics [29]. Materials Studio allows users to build the desired structures and form heterostructures that can be prepared experimentally [30].

3.5.2 Cambridge Serial Total Energy Package (CASTEP)

CASTEP code is an *ab initio* quantum mechanics program designed to simulate solid-state material science interfaces and solid surfaces in a wide range of materials, such as ceramics, semiconductors, metals, and zeolites [31, 32]. The use of first-principle calculations permits researchers to computationally look at the origin, core and nature of electronic, optical and structural properties of the whole structure without any experimental input [33]. Plane-wave pseudopotential calculations are used in CASTEP in the form of a mathematical model of materials. Pseudopotentials in Material Studio replaces the core electrons and an atomic nucleus with the effective numeric potential in the valence electron system [34]. Pseudopotentials and plane waves can be combined to allow the suitable geometry optimizations of interfaces, solids and surfaces. GGA-PBE functionals implemented under Material Studio allows the user to execute valuable calculations of the possible lowest energy cut-off of materials. GGA-PBE are well used in defining the exchange-corrections potentials [35, 36].

3.5.3 Computational Details

First-principles calculations of the individual components and heterostructures were performed using the plane-wave DFT method as implemented in the Cambridge Serial Total Energy Package (CASTEP) code [51] of Material Studio 2019 [52]. The

generalized gradient approximation (GGA) with Perdew-Burke-Ernzerhof (PBE) was used to define the exchange-correlation effect [53]. The plane-wave kinetic energy cut-off was set to be 400 eV for both GaS/C_2N and $GaSe/C_2N$ heterostructures and the individual components. The geometry structures were well relaxed until the energy converged to 10^{-6} eV, where the maximum force of atoms was set to be 0.3 eV/Å, maximum stress to 0.5 GPa and the maximum displacement of the atoms to 0.01 Å. The vdWs corrections in GaS/C_2N heterostructure and the monolayers were treated by applying DFT-D2 method of Grimme [54]. This method has been demonstrated to give a reliable description of the vdW heterostructures [55,56]. The electronic configurations of C ($2s^2$ $2p^2$), S ($3s^2$ $3p^4$), Se ($4s^2$ $4p^4$), N ([He] $2s^2$ $2p^3$), and Ga ($3d^{10}$ $4s^2$ $4p^1$) are treated as the valence electrons. Also, the hybrid Heyd-Scuseria-Ernzerhof (HSE06) [57] functional was to calculate electronic properties since GGA-PBE functional underestimate the bandgap energy of most semiconductors [57]. The Brillouin zone was sampled using Monkhorst-Park *k*-point grid of 5 x 5 x 1 for GaS monolayer, 2 x 2 x 1 for C_2N sheet for the GaS/C_2N heterostructure, 9 × 9 × 1 for GaSe and 4 × 4 × 1 for C_2N sheet for $GaSe/C_2N$ heterostructure were used for the calculation of structural relaxation and electronic properties. To avoid artificial interactions, the two layers are constructed with a large vacuum space of about 20 Å.

3.6 Electronic Properties

In some ways, the semiconductors represent a position between the insulator and metal impurities at a very low temperature, where an impurity can be classified as either acceptor or donor type [37, 38]. Due to the overlapping of bands, the conduction band (CB), as well as the valence band (VB) of a semiconductor consist

of mixed hybrids (s- and p- states) that promote electron-hole pairs [39]. The highest eight (s + p states) split into two separated states, the s and p, each has one s- and three p-states. The lower s-state provides one electron per atom, whereas the three lower p-states can provide three electrons per atom [39].

For a semiconductor to be conductive, electrons have to be excited from the VB into the CB, where an external electric field can accelerate them. The bandgap of the material is an important characteristic due to reduced space can affect the electrical and optical properties of the 2D material [40]. The composition, thickness and stacking order of the heterostructure component depend on the electronic band structure of the layered crystal materials, thus always important to investigate the electronic properties of semiconductors [40].

3.7 The Density of States

The atomic density of state (DOS) provides an insight into the distribution of electron density in or around the Fermi level, and the degree of atomic orbital overlap for each of those systems. The DOS is calculated from the reconstructed dispersion relationship and it plays an important role in determining the density of the semiconductor [41]. The DOS fluctuation represents the creation of an electron-hole pair or electron-electron, with the ground state at T = 0 being a stable combination of the different pair states [42]. The existence of the ground state depends on the interactions between the electron-phonon and electron-electron, which is presented by a potential-dependent interaction in most cases [42]. In several studies, the display of numerical DOS as an energy function for related sets in the superconductor-semiconductor step of the system has been shown [43]. In some instances, the multi-dimensional digitals from the one-dimensional, which was

proposed for the DOS calculations were highly correlated DOS patterns for different metal systems and proposed features to assess the connection between the atomic structures and DOS of the materials in a linear subspace. Where the successful results were reproduced irrespective of the number of electrons in the device.

3.8 The Partial Density of States (PDOS)

The partial density of states (PDOS) gives qualitative insights into the interface electronic structure and identification of the nature of orbitals.The PDOS is traditionally modified by resonance within a device, such as a band structure [44]. It has shown that the nanostructure of a medium can radically change the relationship of dispersion and, thus, allow the manipulation of the PDOS [44]. For a deeper understanding of the nature of the state levels, PDOS is studied concerning the generation of charge carriers in semiconductors [45]. For example, it was found that in TiO_2, the 4s, 2p and 2d atomic shells are responsible for the electron distribution [45]. Furthermore, to understand how O 2p and Ti 3d was involved in the electron movement, the TiO_2 CB was donated by Ti 3d orbital states and the VB by O 2p states [45]. A similar study was done on the ZnO nanostructure to check the PDOS results. In this work, all the O 2p and Zn 3d wave functions are highly localized and the O 2p states are similar to the Zn 3d states, which makes to expect a strong relationship between *p-d* hybridization found to be a strong relationship between O 2p and Zn 3d in ZnO [46].

3.9 Work function

Another factor affecting the properties of improving solar cells is the energy level. It was investigated by calculating the work function (Φ) of the individual monolayers

and the GaS/C_2N heterostructure. The surface conditions of every material can easily affect the work function, which results from altering the surface electric field induced by the distribution of electrons at the interface. The work function is the amount of energy required to remove an electron from the Fermi level surface of a solid to a vacuum at an absolute zero. The work function along the z-axis was calculated by aligning the Fermi energy level concerning the vacuum energy level.

$$\Phi = \mathrm{E_{vacuum}}\text{-}\mathrm{E_{Fermi}} \tag{3.15}$$

where E_{vacuum} and E_{Fermi} are the energy of an electron at the stationary point in the vacuum in line to the surface and Fermi level, respectively. The interface adhesion energy can be calculated by the given equation (3.16):

$$\mathrm{E_{ads}} = \mathrm{E_{A/B}}\text{-}\mathrm{E_A}\text{-}\mathrm{E_B}, \tag{3.16}$$

where $\mathrm{E_A}$, $\mathrm{E_B}$ and $\mathrm{E_{A/B}}$ present the total energies of A and B monolayers, A/B vdW heterostructure.

3.10 Charge carrier mechanism

For any newly formed semiconductor to be considered as valuable for photovoltaic activity, ideally, the bandgap must be within 1.1 to 1.5 eV range to enhance the solar absorption energy. Effective charge separation and optical absorption are also influential in photovoltaic performance. Based on the obtained optical absorption results, there is a good enhancement for visible light for the photovoltaic activity of GaS/C_2N heterostructure and $GaSe/C_2N$ heterostructure compared to the individual materials. The improved photovoltaic activity affected by the efficient separation and transfer of photogenerated electrons depends heavily on the band structures of the individual parts. The GaS/C_2N and $GaSe/C_2N$ heterostructures were assessed by

analysing the band position of the valence band and conduction band concerning the photoexcited electrons of the formed heterostructure. The VBM and CBM of GaS/C_2N and GaSe/C_2N heterostructures were evaluated from the respective bandgaps of the individual components and their absolute electronegativity of atoms using the empirical equations:

$$E_{VB} = X\text{-}E_e + 0.5E_g \quad (3.17)$$

$$E_{CB} = E_{VB}\text{-}E_g \quad (3.18)$$

where X is the standard electrode potential (≃4.5 eV), E_e represents the energy of free electrons of the hydrogen scale and E_g is the estimated bandgap of the studied semiconductor. E_{VB} and E_{CB} represent the conduction band and valence band edge potentials. The X values of C, N, Ga, S and Se are 6.27, 7.30, 3.20, 6.22 and 5.89 eV, respectively. The X values of the C_2N sheet and GaS monolayer were calculated as 4.51 and 4.46 eV, respectively and for GaSe monolayer and C_2N sheet were as follows 4.34 and 4.51 eV, respectively.

3.11 Power Conversion Efficiency Calculations

The power conversion efficiency (PCE) performance of perovskite solar cells has received much attention than the best single-crystalline solar cells. The report was successfully collected and analysed for the operation of photovoltaic cells with their respective power-conversion efficiencies [47]. They clearly show that the PCE of perovskite has been significantly improved from as low as 1.7% PCE that was reported in 2002 by Huynh *et al* [48]. Since the aim is to obtain high PCE for photovoltaic cells, researchers aim to achieve more than 10% PCE. In 2012, about 10% of PCE and higher with different two-dimensional materials was reported [49-52]. The PCE was calculated usingequation 3.19:

$$\eta = \frac{FF.J_{SC}V_{OC}}{P_S} \quad (3.19)$$

where η represents the maximum power conversion efficiency, FF is the fill factor, J_{SC} presents short-circuit current density, V_{OC} is the open-circuit voltage and P_S is the total incident power density, respectively.

The maximum open-circuit voltage (V_o), short circuit current density (J_{sc}) and power conversion efficiency (η) of the formed heterostructure were calculated using Equation 3.20 and 3.21:

$$qV_{OC} = E_G\text{-}E_{loss} \quad (3.20)$$

Subsequently, the relationship between the variable parameter, E_{loss} (adopted with the values of 0.7 eV) and the E_g of the GaS/C_2N heterostructure and GaSe/C_2N heterostructure. The maximum open-circuit voltage (V_o) can be calculated using the above equation.

The following equation can be used to calculate J_{sc},

$$J_{SC} = q\int_{E_g}^{\infty} b_s(E)dE, \quad (3.21)$$

where $b_s(E)$ signify the incident spectral photon flux density and q is the electron charge.

The total incident power density (P_s) is achieved by applying integration normalisation spectral irradiance stated by National Renewable Energy Laboratory (NREL) and is calculated with the following equation:

$$P_s = \int_0^{\infty} Eb_s(E)dE \quad (3.22)$$

Continuous work has taken crystalline silicon (c-Si) cells closer to their theoretical Auger efficiency with a current PCE of 26.6% [53, 54]. Inorganic-organic lead halide perovskite solar cells exhibit a high PCE of about 22.1% [55] at the single-junction,

which is less than the c-Si cells; thus, more focus is needed in improving the power efficiency. However, the dual-junction combination of group III-V materials and Si has so far achieved 32.8% of PCE [56] but due to the costs of group III-V materials, group I have been unable to make it in the market [57].

3.12 Hardware

The computational work was done on the LENGAU High-Performance Computing Cluster, situated at the Centre for High-Performance (CHPC) in Rosebank, Cape Town, South Africa. LENGAU High-Performance Computing Cluster uses a Penta scale system through the DELL server's machines, see Table 3.1.

Table 3.1. Hardware and its parameters.

System Name	Lengau Cluster	FAT Nodes
CPU	Intel ® Xeon ®	Intel ® Xeon ® E7-4850
CPU Clock	2.6 GHz	2.2 GHz
CPU Cores	32832	280
Number of Nodes	1368	5
Memory	148.5 TB	5TB
Rpeak	1.307 TFlops	-
Rmax	1.029 PFlops	-
Interconnect	FDR infiniband Network	-
Shared storage	4 PB Lustre Storage	-
Launch Date	7 June 2016	7 June 2016

https://www.chpc.ac.za/index.php/resources/lengau-cluster

3.13 References

[1] J. Bromberg. The concept of particle creation before and after quantum mechanics. *Hist. Stud. Phys. Sci.* **7** (1976) 161-191.

[2] A. J. Leggett, B. Ruggiero and P. Silvestrini. Quantum Computing and Quantum Bits in Mesoscopic Systems. *Springer*, (2004)

[3] W. De Soto, S. A. Klein and W. A. Beckman. Improvement and validation of a model for photovoltaic array performance. *Sol. Energy* **80** (2006) 78-88.

[4] R. Pariser and R. G. Parr. A Semi-Empirical Theory of the Electronic Spectra and Electronic Structure of Complex Unsaturated Molecules. I. *J. Chem. Phys.* **21** (1953) 466-471.

[5] E. Berardo, L. Turcani, M. Miklitz and K. E. Jelfs. An evolutionary algorithm for the discovery of porous organic cages. *Chem. Sci.* **9** (2018) 8513-8527.

[6] A. D. Becke. Density-functional thermochemistry. I. The effect of the exchange-only gradient correction. *J. Chem. Phys.* **96** (1992) 2155-2160.

[7] P. J. Hasnip, K. Refson, M. I. Probert, J. R. Yates, S. J. Clark and C. J. Pickard. Density functional theory in the solid-state. *Philos. Trans. R. Soc., A* **372** (2014) 28027-28034.

[8] J. Hafner, C. Wolverton and G. Ceder. Toward computational materials design: the impact of density functional theory on materials research. *MRS Bull.* **31** (2006) 659-668.

[9] L. Yang, X. Chen, Z. Qu and J. Gao. Combined Multistate and Kohn-Sham Density Functional Theory Studies of the elusive mechanism of N-dealkylation of N, N-dimethylanilines Mediated by the biomimetic nonheme oxidant Fe^{IV} (O)(N4Py)$(ClO_4)_2$. *Front. Chem.* **6** (2018) 406-415.

[10] R. Baer, E. Livshits and U. Salzner. Tuned range-separated hybrids in density functional theory. *Annu. Rev. Phys. Chem.* **61** (2010) 85-109.

[11] M. T. Lusk and A. E. Mattsson. High-performance computing for materials design to advance energy science. *MRS Bull.* **36** (2011) 169-174.

[12] W. Kohn. Density functional theory. Introductory Quantum Mechanics with MATLAB: For Atoms, Molecules, Clusters, and Nanocrystals (2019)

[13] R. O. Jones. Density functional theory: Its origins, rise to prominence, and future. *Rev. Mod. Phys.* **87** (2015) 897-924.

[14] R. G. Parr. Density functional theory of atoms and molecules. in Horizons of quantum chemistry. *Springer*, (1980), 5-15.

[15] C. Eley, T. Li, F. Liao, S. M. Fairclough, J. M. Smith, G. Smith and S. C. E. Tsang. Nanojunction-Mediated Photocatalytic Enhancement in Heterostructured CdS/ZnO, CdSe/ZnO, and CdTe/ZnO Nanocrystals. *Angew. Chem., Int. Ed.* **53** (2014) 7838-7842.

[16] L. Sham and W. Kohn. One-particle properties of an inhomogeneous interacting electron gas. *Phys. Rev.* **145** (1966) 561.

[17] J. Lahiri and M. Batzill. Surface functionalization of ZnO photocatalysts with monolayer ZnS. *J. Phys. Chem. C* **112** (2008) 4304-4307.

[18] C. Franchini, R. Podloucky, J. Paier, M. Marsman and G. Kresse. Ground-state properties of multivalent manganese oxides: Density functional and hybrid density functional calculations. *Phys. Rev. B* **75** (2007) 195128-195140.

[19] J. P. Perdew, K. Burke and M. Ernzerhof. Generalized gradient approximation made simple. *Phys. Rev. Lett.* **77** (1996) 3865-3869.

[20] Y. Wang and J. P. Perdew. Correlation hole of the spin-polarized electron gas, with exact small-wave-vector and high-density scaling. *Phys. Rev. B* **44** (1991) 13298.

[21] J. P. Perdew, A. Ruzsinszky, J. Tao, V. N. Staroverov, G. E. Scuseria and G. I. Csonka. Prescription for the design and selection of density functional approximations: More constraint satisfaction with fewer fits. *J. Chem. Phys.* **123** (2005) 62201-62211.

[22] J. Perdew, K. Burke and M. Ernzerhof. Perdew, burke, and ernzerhof reply. *Phys. Rev. Lett.* **80** (1998) 891-892.

[23] T. M. Henderson, A. F. Izmaylov, G. E. Scuseria and A. Savin. Assessment of a middle-range hybrid functional. *J. Chem. Theory Comput.* **4** (2008) 1254-1262.

[24] C. Shao, Q. Shao, X. Wang, J. Ling, X. Guo, Y. Ning, Y. Dai, S. Jia, Y. Qiao and C. Li. Supplementary data for the mechanism research for depolymerization of cellulose induced by hydroxyl radical using GC–MS, reaction kinetics simulation and quantum chemistry computation. *Data Brief* (2020) 105329-105340.

[25] D. Systemes. Materials Studio. *BIOVIA, San Diego California, USA* (2014)

[26] L. Zhang, F. Zhang, X. Yang, G. Long, Y. Wu, T. Zhang, K. Leng, Y. Huang, Y. Ma and A. Yu. Porous 3D graphene-based bulk materials with exceptional high surface area and excellent conductivity for supercapacitors. *Sci. Rep.* **3** (2013) 1408.

[27] T. Apple and A. Cutler. The Rensselaer studio general chemistry course. *J. Chem. Educ.* **76** (1999) 462-463.

[28] G. Frison and G. Ohanessian. A comparative study of semiempirical, ab initio, and DFT methods in evaluating metal-ligand bond strength, proton affinity, and interactions between first and second shell ligands in Zn-biomimetic complexes. *J. Comput. Chem.* **29** (2008) 416-433.

[29] P. Sherwood. Hybrid quantum mechanics/molecular mechanics approaches. *Mod. Meth. Algorithms Quantum Chem.* **3** (2000) 285-305.

[30] S. Clark, M. Segall, C. Pickard, P. Hasnip, M. Probert, K. Refson and M. Payne. Materials Studio CASTEP, version 5.0. *Accelrys: San Diego, CA* (2009)

[31] J. C. Tully. Molecular dynamics with electronic transitions. *J. Chem. Phys.* **93** (1990) 1061-1071.

[32] M. Grillo, J. Andzelm, N. Govind, G. Fitzgerald and K. Stark. 10. Computational Materials Science with Materials Studio: Applications in Catalysis. in Computational Materials Science. Springer, 207-221.

[33] S. J. Clark, M. D. Segall, C. J. Pickard, P. J. Hasnip, M. I. Probert, K. Refson and M. C. Payne. First-principles methods using CASTEP. *Z. Kristallogr. Cryst. Mater.* **220** (2005) 567-570.

[34] S.-P. Gao, C. J. Pickard, A. Perlov and V. Milman. Core-level spectroscopy calculation and the plane-wave pseudopotential method. *J. Phys.: Condens. Matter* **21** (2009) 104203-104215.

[35] F. Tran, R. Laskowski, P. Blaha and K. Schwarz. Performance on molecules, surfaces, and solids of the Wu-Cohen GGA exchange-correlation energy functional. *Phys. Rev. B* **75** (2007) 115131-115146.

[36] O. A. von Lilienfeld and P. A. Schultz. Structure and band gaps of Ga-(V) semiconductors: The challenge of Ga pseudopotentials. *Phys. Rev. B* **77** (2008) 115202-115210.

[37] T. Ando, A. B. Fowler and F. Stern. Electronic properties of two-dimensional systems. *Rev. Mod. Phys.* **54** (1982) 437-621.

[38] B. I. Shklovskii and A. L. Efros. Electronic properties of doped semiconductors. *Springer Science & Business Media*, (2013)

[39] R. E. Hummel. Electronic properties of materials. *Springer Science & Business Media*, (2011)

[40] D. K. Sang, B. Wen, S. Gao, Y. Zeng, F. Meng, Z. Guo and H. Zhang. Electronic and Optical Properties of Two-Dimensional Tellurene: From First-Principles Calculations. *Nanomaterials* **9** (2019) 1075-1091.

[41] W. Sturhahn, T. Toellner, E. Alp, X. Zhang, M. Ando, Y. Yoda, S. Kikuta, M. Seto, C. Kimball and B. Dabrowski. Phonon density of states measured by inelastic nuclear resonant scattering. *Phys. Rev. Lett.* **74** (1995) 3832-3836.

[42] V. Händchen, T. Eberle, S. Steinlechner, A. Samblowski, T. Franz, R. F. Werner and R. Schnabel. Observation of one-way Einstein–Podolsky–Rosen steering. *Nat. Photonics* **6** (2012) 596-599.

[43] J. D. Sau and S. D. Sarma. Density of states of disordered topological superconductor-semiconductor hybrid nanowires. *Phys. Rev. B* **88** (2013) 64506-64513.

[44] Z. Jacob, J. Y. Kim, G. V. Naik, A. Boltasseva, E. E. Narimanov and V. M. Shalaev. Engineering photonic density of states using metamaterials. *Appl. Phys. B* **100** (2010) 215-218.

[45] E. M. Kiarii, K. K. Govender, P. G. Ndungu and P. P. Govender. The generation of charge carriers in semiconductors – A theoretical study. *Chem. Phys. Lett.* **678** (2017) 167-176.

[46] C. L. Dong, C. Persson, L. Vayssieres, A. Augustsson, T. Schmitt, M. Mattesini, R. Ahuja, C. L. Chang and J. H. Guo. Electronic structure of nanostructured ZnO from x-ray absorption and emission spectroscopy and the local density approximation. *Phys. Rev. B* **70** (2004) 195325-195330.

[47] M. T. Dang, L. Hirsch and G. Wantz. P3HT:PCBM, Best Seller in Polymer Photovoltaic Research. *Adv. Mater.* **23** (2011) 3597-3602.

[48] W. U. Huynh, J. J. Dittmer and A. P. Alivisatos. Hybrid Nanorod-Polymer Solar Cells. *Science* **295** (2002) 2425.

[49] Z. He, C. Zhong, S. Su, M. Xu, H. Wu and Y. Cao. Enhanced power-conversion efficiency in polymer solar cells using an inverted device structure. *Nat. Photonics* **6** (2012) 591-595.

[50] Y. Liu, C.-C. Chen, Z. Hong, J. Gao, Y. Yang, H. Zhou, L. Dou, G. Li and Y. Yang. Solution-processed small-molecule solar cells: breaking the 10% power conversion efficiency. *Sci. Rep* **3** (2013) 3356-3364.

[51] S.-H. Liao, H.-J. Jhuo, P.-N. Yeh, Y.-S. Cheng, Y.-L. Li, Y.-H. Lee, S. Sharma and S.-A. Chen. Single Junction Inverted Polymer Solar Cell Reaching Power Conversion Efficiency 10.31% by Employing Dual-Doped Zinc Oxide Nano-Film as Cathode Interlayer. *Sci. Rep.* **4** (2014) 6813-6820.

[52] M. M. Lee, J. Teuscher, T. Miyasaka, T. N. Murakami and H. J. Snaith. Efficient Hybrid Solar Cells Based on Meso-Superstructured Organometal Halide Perovskites. *Science* **338** (2012) 643-647.

[53] K. Yoshikawa, W. Yoshida, T. Irie, H. Kawasaki, K. Konishi, H. Ishibashi, T. Asatani, D. Adachi, M. Kanematsu, H. Uzu, and K. Yamamoto. Exceeding conversion efficiency of 26% by heterojunction interdigitated back contact solar cell with thin film Si technology. *Sol. Energy Mater. Sol. Cells* **173** (2017) 37-42.

[54] A. Richter, M. Hermle and S. W. Glunz. Reassessment of the Limiting Efficiency for Crystalline Silicon Solar Cells. *IEEE J. Photovoltaics* **3** (2013) 1184-1191.

[55] W. S. Yang, B.-W. Park, E. H. Jung, N. J. Jeon, Y. C. Kim, D. U. Lee, S. S. Shin, J. Seo, E. K. Kim, J. H. Noh, and S. I. Seok. Iodide management in formamidinium-lead-halide–based perovskite layers for efficient solar cells. *Science* **356** (2017) 1376-1379.

[56] S. Essig, C. Allebé, T. Remo, J. F. Geisz, M. A. Steiner, K. Horowitz, L. Barraud, J. S. Ward, M. Schnabel, A. Descoeudres, David L. Young, M. Woodhouse, M. Despeisse, C. Ballif, and A. Tamboli. Raising the one-sun conversion efficiency of III–V/Si solar cells to 32.8% for two junctions and 35.9% for three junctions. *Nat. Energy.* **2** (2017) 17144-17154.

[57] J. Werner, B. Niesen and C. Ballif. Perovskite/Silicon Tandem Solar Cells: Marriage of Convenience or True Love Story? – An Overview. *Adv. Mate. Interfaces* **5** (2018) 1700731-1700750.

CHAPTER 4:

Tuning the electronic, optical and structural properties of GaS/C_2N van der Waals heterostructure for photovoltaic application: First-Principle Calculations

4.1 Introduction

Globally, the energy demand is escalating with a high rising of renewable sources. Renewable solar energy has been harvested using semiconductors. The use of two-dimensional (2D) semiconductors helps in reducing global pollution and follows green energy production. The 2D semiconductors contain charge mobility carriers, which are the electrons (e^-) in the conduction band (CB) and holes (h^+) in the valence band (VB). There have been different modification methods developed to overcome those existing challenges to improve photovoltaic activities. Amongst other methods, the 2D heterostructure fabrication by coupling two semiconductors to improve the orbital overlapping and staggered valence and conduction bands for the transfer of charge carriers has been a very effective method to overcome these problems. The 2D heterostructure materials surpass the electrons-hole pair's recombination problem and provide visible light trapping through the photogenerated electrons.

Carbon nitride (C_2N) is one of the most promising photovoltaic materials due to its low-cost, high stability, visible-light region and its availability as an abundant material. Previous reports articulate that the transfer of photogenerated electrons in

The work presented in this chapter was published in *SN Applied Sciences* **2** (2019) 341.

the C_2N layer are not well separated and transported from the CB to the VB. Thus, the C_2N layer promotes the fast recombination of photogenerated electrons, thereby reducing the visible light absorption efficiency. To overcome these issues, the C_2N layer can be coupled with another effective semiconductor to improve its ability to trap visible light for photovoltaic activity. To boost the C_2N layer performance, gallium sulphide (GaS) semiconductor was used. A GaS semiconductor has an experimental bandgap of 2.59 eV [1]. The GaS semiconductor is considered a promising material close to blue light-emitting devices [2]. Moreover, the GaS semiconductor reveals the capability of electroluminescence and photoluminescence region, due to understanding carrier connections to the photogenerated electron-hole pairs recombination [3].

In this work, GaS/C_2N van der Waals (vdWs) heterostructure was evaluated as a suitable photovoltaic material through Density Functional Theory (DFT) method by calculating the geometrical structure, electronic properties, the total projected density of states, work function, charge density difference, Mulliken charge population, optical properties and light power conversion efficiency.

4.2 COMPUTATIONAL DETAILS

The computational details, including the geometry optimization, optical property and electronic structure calculation, were calculated as detailed in Chapter 3.

4.3 Results and discussion

4.3.1 Geometry structures

We begin with the calculations of the proposed 2D semiconductors, focusing on the geometry structural and electronic bandgap properties of the individual materials. The individual structures of GaS and C_2N are shown in Figure 4.1.

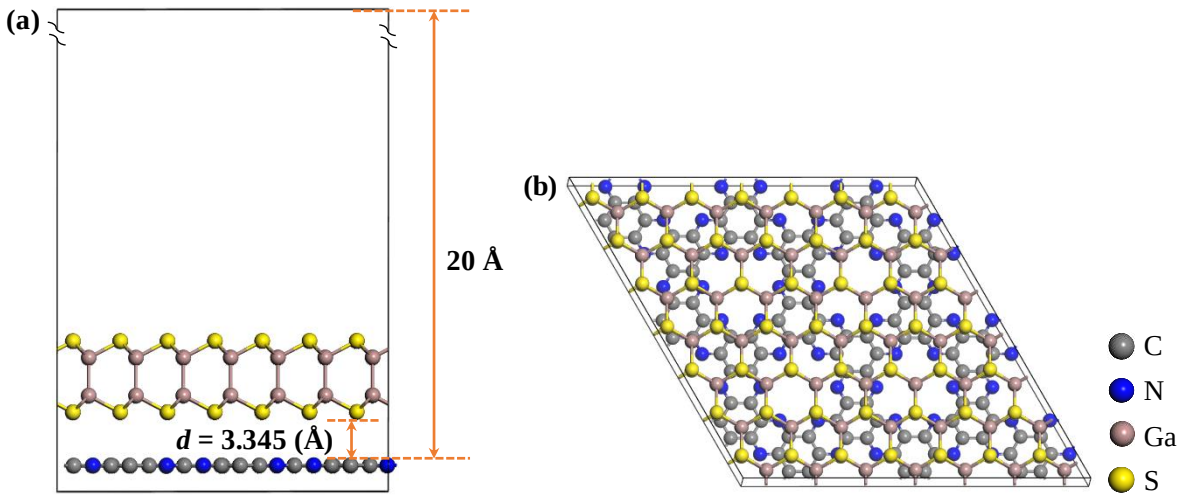

Figure 4.1. The optimized stable geometry (a) side and (b) top views of GaS/C_2N heterostructure.

The unit cell of C_2N sheets consists of 6 nitrogen atoms and 12 carbon atoms with uniform holes. The calculated optimized lattice constant parameters of C_2N sheet and GaS monolayer were *a* = 8.33 and b = 3.57 Å (see Table 4.1), respectively, as with the previous lattice constant parameters of 8.32 Å (C_2N) and 3.58 Å (GaS) [4, 5].

Table 4.1. The calculated lattice parameter, binding energy (E_b) and interface distance (*d*) for C_2N, GaS and GaS/C_2N.

	Lattice parameters (Å)				
Semiconductors	*a*	*b*	*c*	E_b(meV)	*d*(Å)
C_2N	8.33	8.33	27.00	-	-
GaS	3.57	3.57	24.67	-	-
GaS/C_2N	25.75	25.75	28.45	-0.069	3.345

The bond lengths of C-N (1.34 Å), C-C_1 (1.43 Å) and C-C_2 (1.47 Å) were consistently agreeing with previously reported bond lengths of 1.34, 1.43 and 1.47 Å [6-8], respectively. The bond angle of 117.7º for C-N-C slightly deviates from that obtained by Liang *et al.* [62]. The obtained bond length of Ga-S was 2.43 Å, whereas Ga-Ga was 2.54 Å, which also agreed very well with previous studies (2.327 and 2.451 Å for Ga-S and Ga-Ga, respectively) [9].

The top and side views of the optimized GaS/C_2N heterostructure are shown in Figure 4.1(a) and (b), respectively. The geometry structure of C_2N sheet maintains its uniform planar structure with no distortion within its structure. Moreover, GaS monolayer also remains with its linear structure. The lattice constants parameters of GaS/C_2N heterostructure were a = b = 25.75 Å (Table 4.1). The equilibrium distance between the optimized structures of C_2N sheet and the GaS monolayer was measured as 3.345 Å (Table 4.1), which is close to the C_2N bilayer with a good stacking order distance of 3.280 Å [4]. To check the stability between the GaS monolayer and C_2N sheet, the binding energy (E_b)of the GaS/C_2N heterostructure geometric were calculated. An E_b value of -0.069 meV was calculated; this suggests that C_2N/GaS heterostructure is energetically favourable.

4.3.2 Electronic properties

The electronic band structures of GaS/C_2N heterostructure, GaS and C_2N composites were studied to understand their photovoltaic performance. Furthermore, the projected density of state (PDOS) was also evaluated to gain more knowledge on the classification of the nature of orbitals and electronic structural interface. The obtained outcome of the electronic band structures and PDOS are shown in Figures 4.2 and 4.3, respectively.

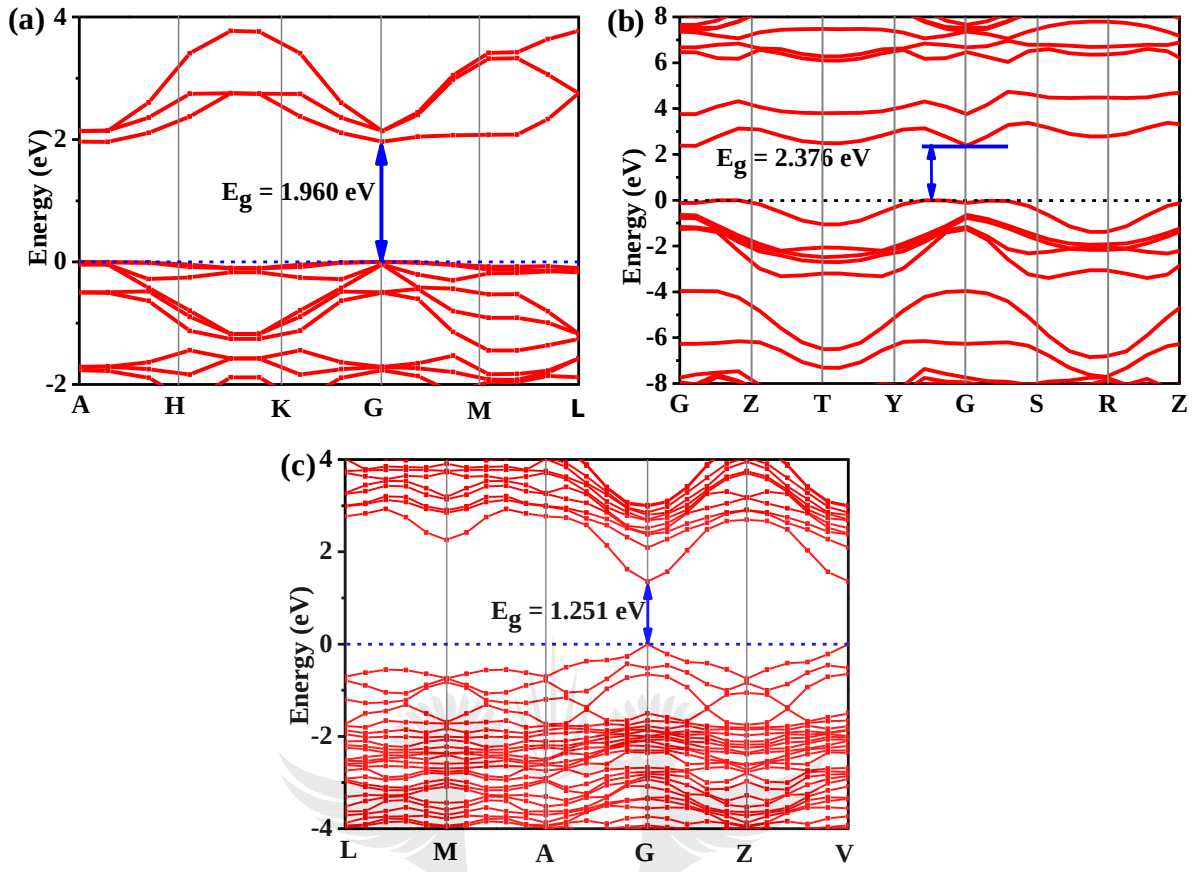

Figure 4.2. The calculated band structures for (a) C_2N layer, (b) GaS monolayer and (c) GaS/C_2N heterostructure.

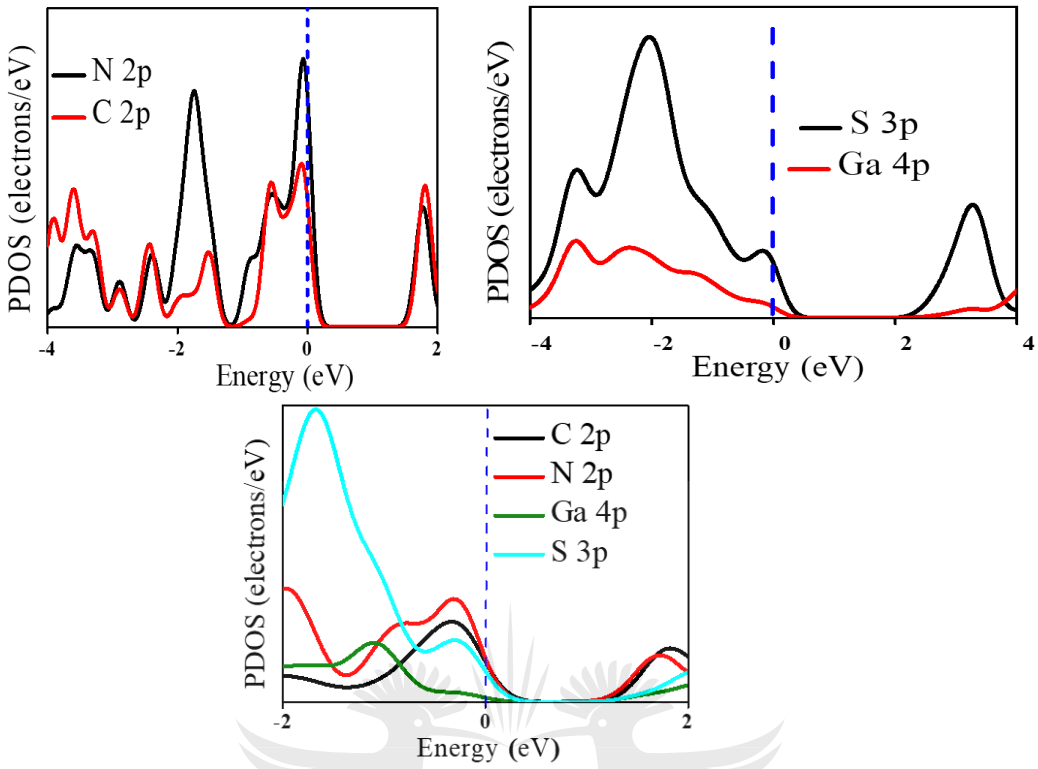

Figure 4.3. The calculated projected density of state of (a) C_2N layer, (b) GaS monolayer and (c) GaS/C_2N heterostructure are presented.

Figure 4.3 (a) shows a C_2N sheet band edges were dominated by the C *2p* and N *2p* states [10]. The CBM and VBM were both located at the Fermi level (*G* point), which makes C_2N monolayer a direct electronic bandgap material with bandgap energy (E_g) of 1.96 eV and this was in good agreement with previously reported studies [11]. GaS monolayer showed an indirect electronic bandgap of about 2.38 eV (Figure 4.2 (b)), which was in good agreement with the experimental value of 2.59 eV [1] with a variation of about 0.21 eV.

The PDOS results confirmed that Ga 4p and S 3p states contribute more to the CBM of GaS monolayer, see Figure 4.3 (b). The CBM for GaS was positioned between the *Y*-*G* points, whereby the VBM was at (Fermi level) *G* point. The VBM and CBM of GaS were mostly dominated by S *3p* state.

The electronic band structures of C_2N sheet and the GaS monolayer were greatly reduced by forming a GaS/C_2N vdW heterostructure,see Figure 4.3 (c) . The absorption light-harvesting heterostructure with 1.2-1.5 eV narrow bandgap is the supreme efficiency according to the Shockley-Queisser range [12]. Consequently, the reduced electronic bandgap of GaS/C_2N heterostructure could be useful in enhancing the light absorption of photovoltaic cells. The direct electronic bandgap of GaS/C_2N heterostructure is fundamental to its optoelectronic application performance [13] as it favours optical transition with significant changes in the wave vector, thus improving the visible light response.

The photogenerated charge carriers of an indirect gap semiconductor change their momentum state before electron-hole pairs recombination due to phonon emission occurrence [14]. The obtained direct electronic bandgap nature of GaS/C_2N vdW heterostructure (1.25 eV) in Figure 4.2 (c) is within the acceptable range of 1.1 to 1.5 eV, which is the recommended electronic bandgap range for PV cells [1, 15, 16]. Therefore, the electronic bandgap could lead to the improved harvesting of visible light. While the optical transitions through the indirect electronic bandgap nature of a heterostructure are not recommended; thus, the materials are not efficient light emitters for photovoltaic cells [17]. The band alignment of C_2N sheet and GaS monolayer formed a type-I heterostructure (Figure 4.7). The GaSe monolayer will have a low electron-hole pairs generation when exposing to visible light beavuse on the greater bandgap than C_2N sheet. As the GaS/C_2N heterostructure was exposed to visible light, the electrons were photo-generated from the CB of GaS monolayer to CB of C_2N sheet.

4.3.3 Work function

The calculated work function for C_2N sheet, GaS monolayer and GaS/C_2N vdW heterostructure was estimated to be 5.79 eV, 6.04 eV and 5.65 eV, respectively, see Figure 4.4.

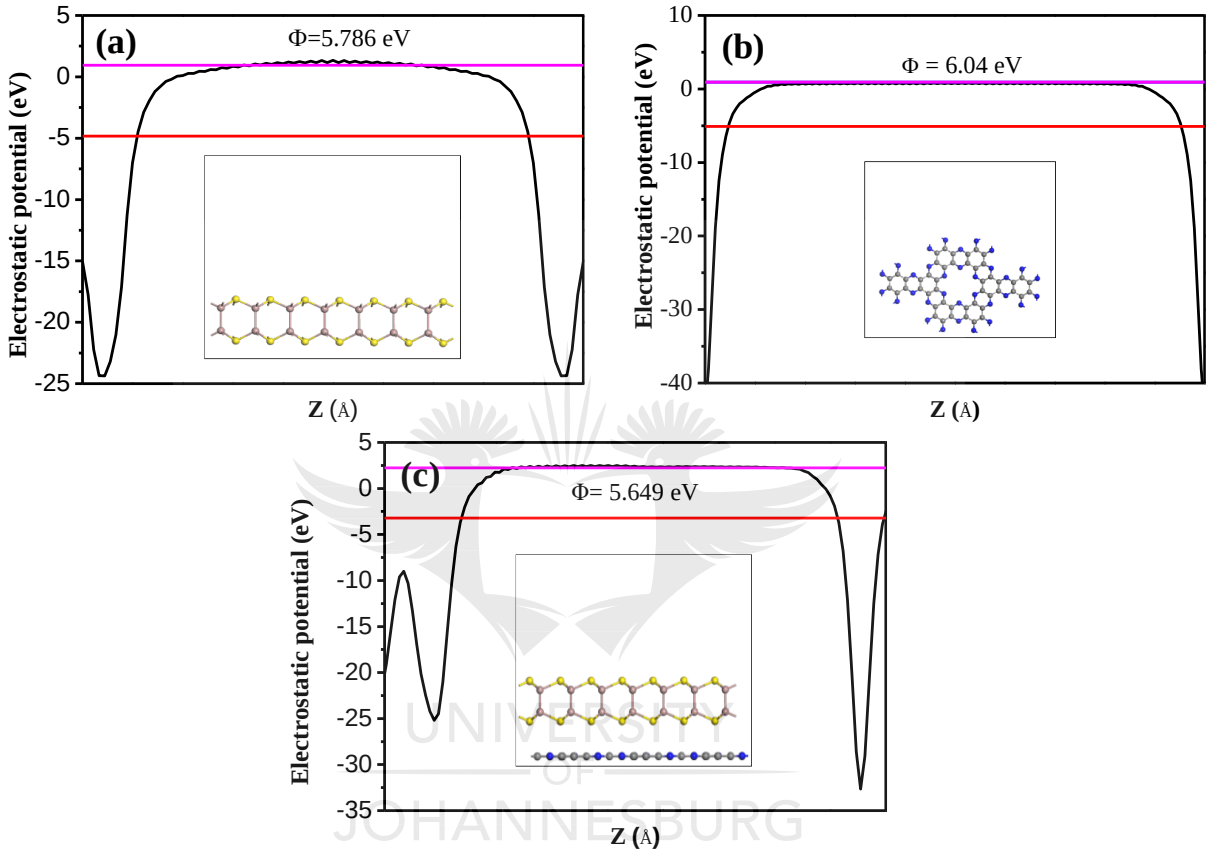

Figure 4.4. The calculated work function for (a) GaS monolayer, (b) C_2N sheet and (c) GaS/C_2N heterostructure.

The determined work function of GaS monolayer (5.79 eV) and C_2N sheet (6.04 eV) displayed reduced energy compared with the reported theoretical results of 6.10 eV for GaS monolayer and 6.18 eV for C_2N sheet [5, 18]. The work function difference for GaS monolayers was 0.31 eV and for C_2N sheets was 0.14 eV, respectively. The C_2N sheet seems to have a higher work function than the GaS monolayer due to the high ionization energy of the N atom compared to the S atom [19]. Therefore,

the GaS monolayer with a lower work function could determine the electron charge transfer at the interface level. Hence, the electrons could transfer from GaS monolayer to C_2N sheet with a significantly lower work function. In this case, the C_2N sheet would be a negatively charged semiconductor, while GaS would be a positively charged semiconductor due to the high electrostatic induction.

The calculated work function of GaS/C_2N heterostructure was found to be 5.65 eV due to the impact of electron charge transfer and interfacial formation [20]. A very low work function suggests that low energy would be needed to excite electrons from the VBM to CBM edges; thus, more electrons would be transferred. The associated phenomenon is that the work function is directly proportional to the kinetic energy of an electron. Furthermore, the electrostatic potential difference at the GaS/C_2N heterostructure interface edges successfully decreases, the electrons and holes recombination rate, increase the electron charge transfer and separation of the induced charge carriers which could improve performance of power conversion efficiency.

4.3.4 Charge density difference

To check the electron charge transfer between the C_2N sheet and GaS monolayer, which signifies the charge distribution between the two semiconductors charge density difference is calculated. To further understand, we checked the charge transfer of GaS/C_2N heterostructure, a three-dimensional (3D) charge density difference was evaluated with an isosurface valued of 0.003 e/Å^3, as shown in Figure 4.5.

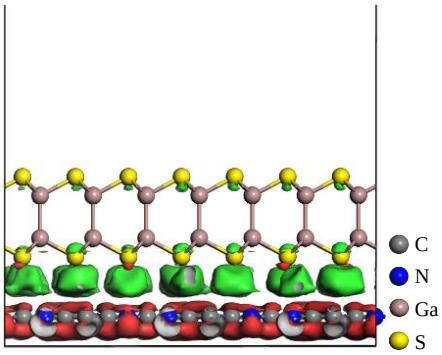

Figure 4.5. A GaS/C_2N heterostructure 3D charge density difference is represented. The red and green areas signify charge accumulation and depletion, respectively.

A high charge accumulation of electrons was found on the C_2N edges, whereas depletion occurred at the GaS monolayer edges. The red region predicts that the electrons are rich in the GaS monolayer, making GaS monolayer an electron-rich semiconductor. In this case, C_2N sheet acts as a hole-rich semiconductor. Therefore, we expect electrons to move from the GaS monolayer surface to the C_2N surface. Subsequently, GaS monolayer acts as a photosensitizer in GaS/C_2N heterostructure. Therefore, this improves the distribution of charge density and the separation of electron-hole pairs within the GaS/C_2N heterostructure.

The Mulliken charge population analysis report shows the total amount of electron charge transferred at the GaS/C_2N vdW heterostructure surface to be 0.13 |*e*|. The S atoms have about -0.43 |*e*| of average contribution. Notwithstanding, GaS monolayer contributes about -0.02 |*e*| charge population. Therefore, C_2N monolayer receives an average of 0.13 |*e*|; thus making the N atom receive more electrons in the GaS/C_2N heterostructure with an average amount of about -0.31 |*e*|. The charge population distribution at the interface could help tune the electrostatic potential to

improve photovoltaic light detection and harvesting. The electron charge transfer at GaS/C_2N heterostructure surface shows that the formation could accomplish strong orbital overlapping, leading to a high efficient electron charge transfer for photovoltaic activity.

4.3.6 Optical properties

A good performing photovoltaic material should absorb a high-intensity amount of visible light to achieve an efficient electric current conversion. The calculated optical property of GaS/C_2N heterostructure, C_2N sheet and GaS monolayer was studied through UV-visible light absorption spectrum. A redshift of the absorption of GaS/C_2N heterostructure showed an enhancement because of the reduced indirect bandgap compared with GaS and C_2N counterparts, as shown in Figure 4.6.

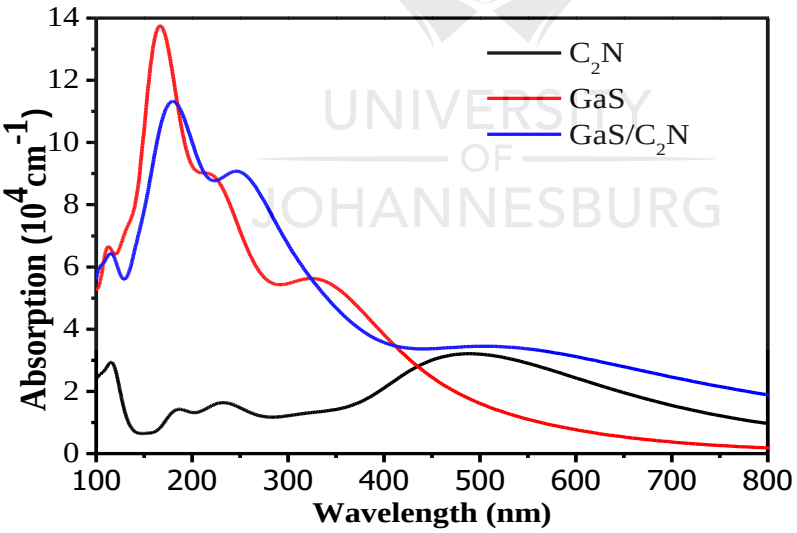

Figure 4.6. The calculated light absorption spectrum of GaS/C_2N heterostructure, GaS monolayer and C_2N sheet.

Comparing C_2N sheet and GaS monolayer, the absorption edges moved to the wider wavelength region for GaS/C_2N heterostructure due to the merging C_2N sheet

and GaS monolayer. The results compared well to bandgap individual semiconductors (C_2N sheet and GaS monolayer) with significantly poor visible light absorption capacity [21, 22], whereby GaS/C_2N heterostructure reveals more absorption intensity in the wide range of spectra 410-800 nm. In this work, the data predicted that the optical properties and the stability of GaS/C_2N heterostructure could improve the visible light absorption. This means GaS/C_2N heterostructure can be used in photovoltaic devices for the conversion of solar energy to electrical current.

4.3.7 Charge carrier mechanism

To assess the visible light absorption performance, the E_{VB} and E_{CB} for C_2N were calculated as 0.99 eV and -0.97 eV, respectively. Furthermore, the corresponding band edges of GaS monolayer were calculated as 1.15 and -1.23 eV, respectively. This band alignment demonstrates that the CB and VB GaS were much higher than that of C_2N, respectively. The possible transfer of charge electrons was proposed for GaS/C_2N heterostructure based on the proposed band edges mechanism, as shown in Figure 4.7.

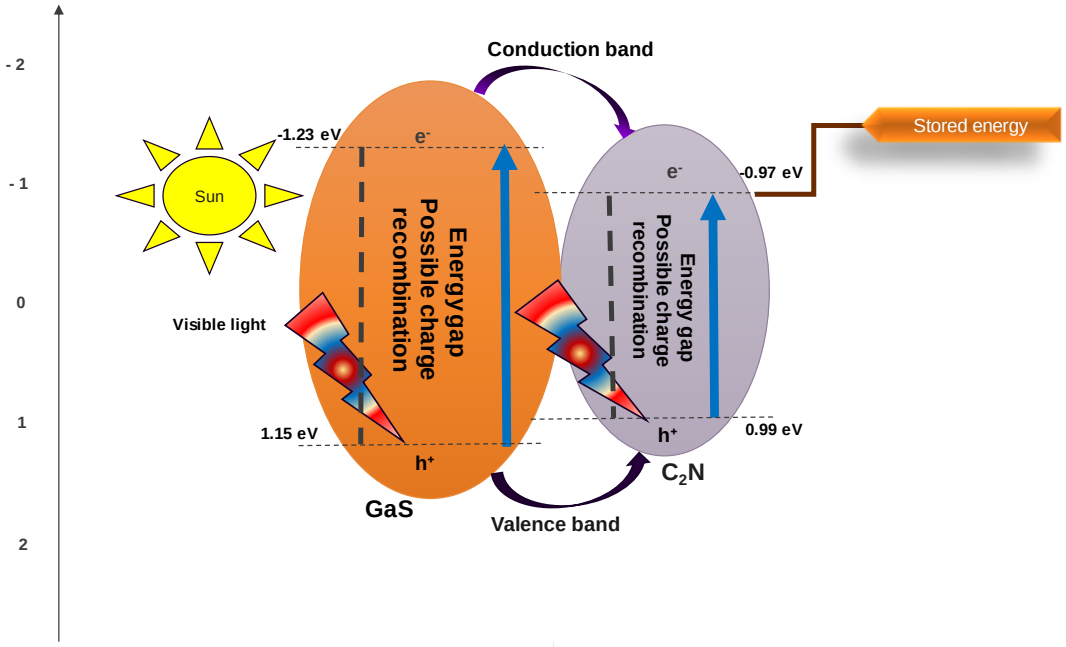

Figure 4.7. Schematic band alignment presentation of the conduction band and valence band of GaS monolayer and C_2N sheet.

The photo-generated electron-hole pairs in the CB and VB, respectively, of the GaS monolayer, could make electrons transfer to the C_2N sheet. The band alignment mechanism in Figure 4.7 forms a type-I heterostructure formation. The VB (0.99 eV) of C_2N sheet are higher than the VB (1.15 eV) of GaS monolayer. Furthermore, the CB (-1.23 eV) of C_2N sheet are lower than the CB (-0.97 eV) of GaS monolayer. The type-I band alignment of GaS/C_2N heterostructure could promise better harvesting of sunlight and transfer of electron charge carriers [23].

4.4 Power conversion efficiency (PCE)

In the 2D GaS/C_2N heterostructure, the decrease of electron bandgap, outstanding electron-hole pairs transport properties and absorption optical enhancement provides more effectiveness in increasing the power conversion efficiency. GaS/C_2N heterostructure could improve the photovoltaic performance since both V_{oc} and J_{SC}

results in a high PCE of about 17.8%. This suggests that GaS/C_2N heterostructure could be an ideal material in a photovoltaic device.

4.5 Conclusion

The obtained electronic properties of GaS/C_2N heterostructure showed a reduced indirect electron bandgap of 1.251 eV compared to the GaS monolayer and C_2N sheet counterparts. The proposed 2D GaS/C_2N vdW heterostructure exhibited a significantly wider visible-light absorption edge with a lower work function of 5.65 eV, which was lower than GaS monolayer and C_2N sheet of 5.79 eV and 6.04 eV, respectively. The GaS/C_2N vdWs heterostructure showed a high PCE of 17.8 %. The results predicted that the 2D GaS/C_2N vdWs heterostructure could be an appropriate replacement for lead-containing materials to reduce the effects of greenhouse gases that impose on the environment and human health.

4.6 Reference

[1] E. Aulich, J. Brebner and E. Mooser. Indirect energy gap in GaSe and GaS. *Physica Status Solidi (b)* **31** (1969) 129-131.

[2] F. Ponce and D. Bour. Nitride-based semiconductors for blue and green light-emitting devices. *Nature* **386** (1997) 351-359.

[3] Y. Honmou, S. Hirata, H. Komiyama, J. Hiyoshi, S. Kawauchi, T. Iyoda and M. Vacha. Single-molecule electroluminescence and photoluminescence of polyfluorene unveils the photophysics behind the green emission band. *Nat. Commun.* **5** (2014) 1-8.

[4] Z. Guan and S. Ni. Insights from first principles graphene/gC_2N bilayer: gap opening, enhanced visible light response and electrical field tuning band structure. *Appl. Phys. A* **123** (2017) 678.

[5] M. Yagmurcukardes, R. Senger, F. Peeters and H. Sahin. Mechanical properties of monolayer GaS and GaSe crystals. *Phys. Rev. B* **94** (2016) 245407-245414.

[6] J. Du, C. Xia, W. Xiong, X. Zhao, T. Wang and Y. Jia. Tuning the electronic structures and magnetism of two-dimensional porous C_2N via transition metal embedding. *Phys. Chem. Chem. Phys.* **18** (2016) 22678-22686.

[7] Y. Xu, B. Peng, H. Zhang, H. Shao, R. Zhang and H. Zhu. First-principle calculations of optical properties of monolayer arsenene and antimonene allotropes. *Ann. Phys.* **529** (2017) 1600152-1600169.

[8] Z. Guan, C.-S. Lian, S. Hu, S. Ni, J. Li and W. Duan. Tunable structural, electronic, and optical properties of layered two-dimensional C_2N and MoS_2 van der waals heterostructure as photovoltaic material. *J. Phys. Chem. C* **121** (2017) 3654-3660.

[9] W. Wei, Y. Dai, C. Niu, X. Li, Y. Ma and B. Huang. Electronic properties of two-dimensional van der Waals GaS/GaSe heterostructures. *J. Mater. Chem. C* **3** (2015) 11548-11554.

[10] X. Wang, R. Quhe, W. Cui, Y. Zhi, Y. Huang, Y. An, X. Dai, Y. Tang, W. Chen and Z. Wu. Electric field effects on the electronic and optical properties in C_2N/Sb van der Waals heterostructure. *Carbon* **129** (2018) 738-744.

[11] P.-P. Sun, Q.-S. Li, S. Feng and Z.-S. Li. Mixed Ge/Pb perovskite light absorbers with an ascendant efficiency explored from theoretical view. *Phys. Chem. Chem. Phys.* **18** (2016) 14408-14418.

[12] W. Shockley and H. J. Queisser. Detailed balance limit of efficiency of p-n junction solar cells. *J. Appl. Phys.* **32** (1961) 510-519.

[13] R. A. Soref. Silicon-based optoelectronics. *Proc. IEEE* **81** (1993) 1687-1706.

[14] F. Opoku, K. K. Govender, C. G. C. E. van Sittert and P. P. Govender. Role of MoS_2 and WS_2 monolayers on photocatalytic hydrogen production and the pollutant degradation of monoclinic $BiVO_4$: A first-principles study. *New J. Chem.* **41** (2017) 11701-11713.

[15] P. D. Antunez, J. J. Buckley and R. L. Brutchey. Tin and germanium monochalcogenide IV–VI semiconductor nanocrystals for use in solar cells. *Nanoscale* **3** (2011) 2399-2411.

[16] D. J. Wehenkel, K. H. Hendriks, M. M. Wienk and R. A. Janssen. The effect of bias light on the spectral responsivity of organic solar cells. *Org. Electron.* **13** (2012) 3284-3290.

[17] L.-D. Yuan, H.-X. Deng, S.-S. Li, S.-H. Wei and J.-W. Luo. Unified theory of direct or indirect band-gap nature of conventional semiconductors. *Phys. Rev. B* **98** (2018) 245203-245218.

[18] W. Xu, C. Chen, C. Tang, Y. Li and L. Xu. Design of Boron Doped C_2N-C_3N Coplanar Conjugated Heterostructure for Efficient HER Electrocatalysis. *Sci. Rep.* **8** (2018) 1-9.

[19] X. Tan, L. Kou, H. A. Tahini and S. C. Smith. Conductive graphitic carbon nitride as an ideal material for electrocatalytically switchable CO_2 Capture. *Sci. Rep.* **5** (2015) 1-8.

[20] K. M. Alam, P. Kumar, P. Kar, U. K. Thakur, S. Zeng, K. Cui and K. Shankar. Enhanced charge separation in gC_3N_4–BiOI heterostructures for visible light driven photoelectrochemical water splitting. *Nanoscale Adv.* **1** (2019) 1460-1471.

[21] F. Zeng, W.-Q. Huang, J.-H. Xiao, Y.-y. Li, W. Peng, W. Hu, K. Li and G.-F. Huang. Isotype heterojunction g-C_3N_4/g-C_3N_4 nanosheets as 2D support to highly dispersed 0D metal oxide nanoparticles: generalized self-assembly and its high photocatalytic activity. *J. Phys. D: Appl. Phys.* **52** (2018) 25501-25529.

[22] H.-Y. Wu, K. Yang, Y. Si, W.-Q. Huang, W. Hu, P. Peng and G.-F. Huang. Interfacial interaction between Boron cluster and metal oxide surface and its effects: a case study of B_{20}/Ag_3PO_4 van der Waals Heterostructure. *J. Phys. Chem. C* **122** (2018) 6151-6158.

[23] X. Jia, J. Cao, H. Lin, M. Zhang, X. Guo and S. Chen. Transforming type-I to type-II heterostructure photocatalyst via energy band engineering: a case study of I-BiOCl/I-BiOBr. *Appl. Catal., B* **204** (2017) 505-514.

CHAPTER 5:

Exploring the Optical, Structural and Electronic Properties of Two-Dimensional GaSe/C_2N van der Waals Heterostructure as Photovoltaic Cell: A Computational Investigation

5.1 Introduction

Solar energy is currently the most reliable, harmless and clean energy so far, and photovoltaic (PV) energy generation is one of the effective ways of utilizing solar energy throughout the world [1]. In this global energy and environment crisis, we are facing, PV power generation has been vital in energy emissions reduction and energy saving. Photovoltaic generation can assist the recent demand for electrical energy and increased electrified cooling, heating and transport, so it has sound compensations for achieving the sustainability and environmental friendliness aims of energy policy at very low-costs [2].

With the recent technological improvements and techniques, photovoltaic power generation has had magnificent advanced growth in the whole world [3, 4]. It has shown an increase in the installation of about 110 Gigawatt (GW) in the ending year of 2016 [4]. The projected aim is to reach 400 GW by 2030 ending year [5]. This clearly shows that there is great hope of fast growth for photovoltaic power generation for future use. The entire world has recognized the value of photovoltaic power generation through its ability to safe energy and toxic gases emission reduction [6].

The work presented in this chapter was published in the Journal of Electronic Materials.

The PV cells industry has been explosively developed based on a combination of two-dimensional (2D) materials. The current hybrid organic-inorganic 2D materials have shown excellent properties for harvesting high efficient visible light for photovoltaic generation, with advantages such as high electronic mobility [7], tunable bandgap [8] and large visible-light absorption coefficients [9]. Power conversion efficiency (PCE) of about 22% using thin-film and polycrystalline perovskite materials has been reported [10].

The perovskite materials having higher power conversion efficiency (PCE) contains the excess of heavy metal elements, such as lead (Pb), which are very harmful to humans and the environment [11]. However, 2D materials, such as germanium (Ge) and gallium (Ga), are considered more stable than lead-containing materials. So far there have been many different 2D materials, such as carbon-nitride (C_2N) [12], C_3N_4 [13], C_6N_6 [14] and transition metal dichalcogenides [15, 16], which are broadly used in PV cells. Lately, 2D C_2N has shown a lot of interest in the field of photovoltaics due to its economic affordability, chemical stability, earth-abundant nature, high thermal and tunable electronic structure [17]. These properties make C_2N to be a very promising material for solar energy conversion. Density functional theory (DFT) theory has been used to study the light absorption of C_2N [10]. In C_2N, the benzene rings are bridged by pyrazine rings consisting of six-member D_{2h} rings with two nitrogen atoms facing each other. The prepared field-effect transistor based on the C_2N multilayer has a high on/off ratio of 10^7 [18].

For the C_2N sheet to perform well, it will require an improvement of another 2D material for electronic structure tuning [19]. The formation of heterostructure materials was used to improve the absorption of light emitted for photovoltaic cells,

to generate sufficient energy to be converted into electrical energy [20]. To enhance the light-absorbing ability of C_2N sheet, the GaSe monolayer was coupled with the C_2N sheet. In this work, we investigate in detail the theoretical study of GaSe/C_2N van der Waal heterostructure by calculating the electronic, structural and optical properties. The obtained results may help the design and application of GaSe/C_2N heterostructure as a visible-light photovoltaic device [21].

5.2 COMPUTATIONAL DETAILS

The computational details, including the geometry optimization, optical property and electronic structure calculation, were done as detailed in Chapter 3.

5.3 Results and Discussion

5.3.1 Geometry structures

To have more understanding of the proposed GaSe/C_2N vdW heterostructure, the electronic properties and geometric structure of the suggested 2D semiconductors were firstly evaluated. Similarly, with the structure of graphene, the C_2N sheet was formed by a hexagonal arrangement with large pores, as presented in Figure 5.1.

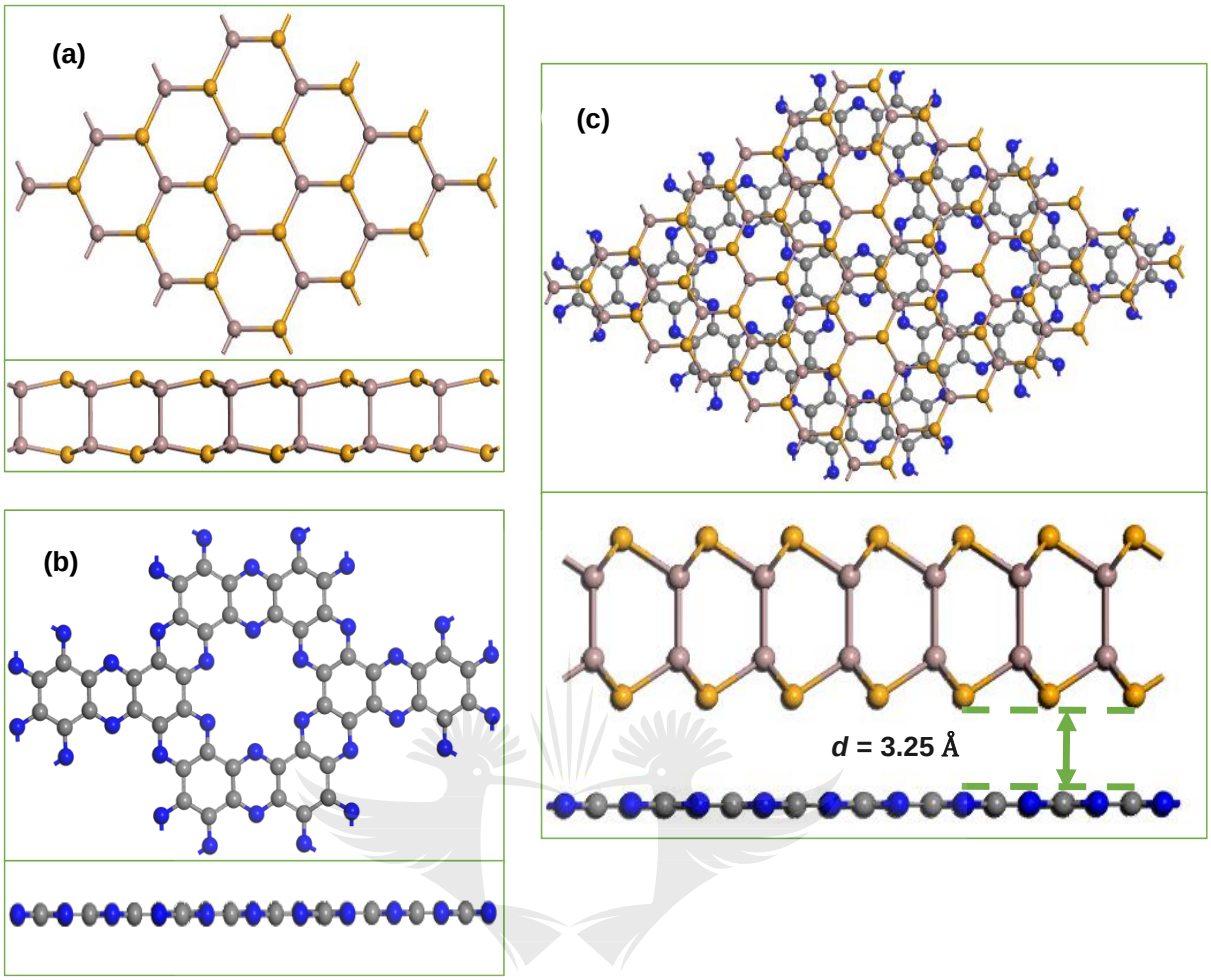

Figure 5.1. Optimized geometrical structure of (a) GaSe monolayer, (b) C_2N sheet and (c) GaSe/C_2N vdW heterostructure. The blue, dark grey, gold and light grey represent the N, C, Se and Ga atoms, respectively.

An individual C_2N sheet consists of two different C-N and C-C bonds. The calculated bonds length of C-C and C-N were found to be 1.337 and 1.431 Å, respectively. The weak atomic thin layer allows the formation of several interactions within the semiconductor, which has two sheets of Ga layer double-decker between chalcogenide layers as Se-Ga-Ga-Se. The lattice parameters of C_2N sheet were determined to be $a = b = 8.33$ Å and $\gamma = 120^{o}$ (Table 5.1), which agreed very well with the previous experimental data [22, 23]. The lattice constrains parameters of

GaSe monolayer was determined to be $a = b = 3.77$ Å and $\gamma = 120^o$, which was in agreement with previous results [24].

Table 5.1. The calculated lattice constraint parameters, binding energy (E_b) and interfaces distance (d) for C_2N, GaSe and GaSe/C_2N.

	Lattice constraints parameters (Å)				
Semiconductors	*a*	*b*	*c*	E_b(meV)	*d*(Å)
C_2N	8.33	8.33	27.00	-	-
GaSe	3.77	3.77	24.97	-	-
GaSe/C_2N	15.88	15.88	28.89	-0.089	3.25

The side and top views of C_2N sheet, GaSe monolayer and GaSe/C_2N vdW heterostructure are represented in Figure 5.1. (a)-(c), respectively. The distance between C_2N sheet and GaS monolayer were found to be about 3.25 Å apart. The binding energy (E_b) of -0.089 eV was found, which shows that the formed GaS/C_2N vdW heterostructure was exothermic. The weak van der Waals force slab interaction plays a critical role in explaining the non-bond interaction in the layered materials.

5.3.2 Electronic structures

To explore the effects of electric field on the electronic band structures, the electronic band structure of GaSe monolayer, C_2N sheet and GaSe/C_2N van der Waals heterostructure were calculated. The results reveal the effect of interfacial interaction on electronic band structure properties for photovoltaic performance. The bandgap results are shown in Figure 5.2.

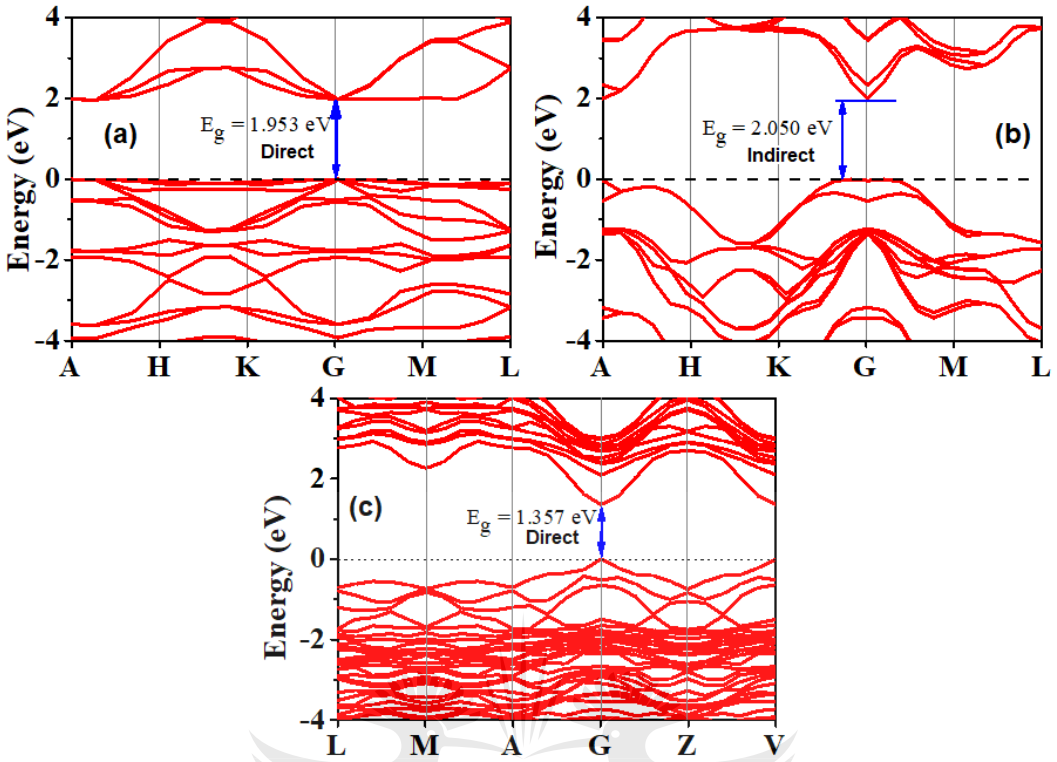

Figure 5.2. Electronic band structures of (a) C_2N sheet, (b) GaSe monolayer and (c) GaSe/C_2N. The Fermi level is set to be zero.

Since conduction band minimum (CBM) and valence band maximum (VBM) are positioned within the *G*-point, this confirms direct bandgap of C_2N sheet. The band structure in Figure 5.2 (a) indicates that the C_2N sheet exhibited p-type electrical characteristic with a direct bandgap of 1.953 eV, which was relatively lower than the experimental band gap of 1.96 eV, having a slight difference of about 0.007 eV [25]. In Figure 5.2(b), GaSe monolayer was calculated and showed an indirect bandgap of about 2.050 eV, which was close to the reported value of 2.1 eV [26] with a difference of 0.05 eV. In GaSe monolayer, the CBM is positioned on the G-point, while VBM is positioned between *K-G* and *G-M* points, thus making GaSe monolayer an indirect bandgap semiconductor.

A bandgap of about 1.357 eV was calculated for GaSe/C_2N vdW heterostructure. Due to the interfacial interaction of GaSe monolayer and C_2N sheet, the bandgap of GaSe/C_2N vdW heterostructure has been reduced effectively compared to those of GaSe monolayer and C_2N sheet counterparts.

The theoretical simulation has shown that the direct bandgap of 1.357 eV from Figure 5.2© was within the range for a photovoltaic cell (1.1-1.5 eV) [27]. Therefore, this suggests more of the solar spectrum can be converted into electricity. Moreover, it was quite evident that C_2N sheet electronic bandstructure was not destroyed as the electronic bandgap of C_2N/GaSe heterostructure was a direct bandgap, which could be attributed to the weak interaction in GaSe/C_2N vdW heterostructure.

5.3.3 Partial density of states (PDOS)

The partial density of states analysis gives us an insight into the distribution of the electronic density near or at the Fermi level. The PDOS analysis also explains the atomic orbital overlapping for the GaSe/C_2N vdW heterostructure system. The PDOS analysis results are shown in Figure 5.3.

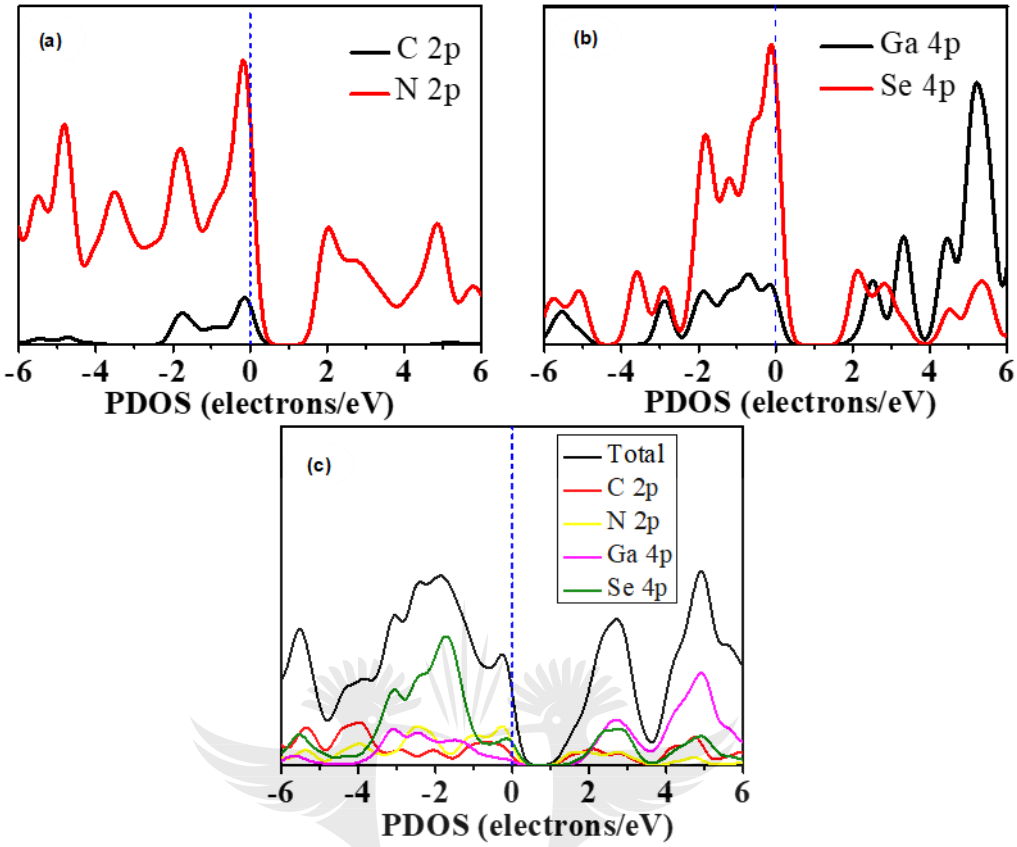

Figure 5.3. Calculated of the partial density of states for (a) C_2N sheet, (b) GaSe monolayer and (c) GaSe/C_2N vdW heterostructure. The Fermi level is set to be zero as a vertical dashed line.

Based on the PDOS results, Figure 5.3 clearly shows that GaSe/C_2N vdW heterostructure bandgap was breaking near the Fermi level representing the nature of the semiconductor [28]. The PDOS confirmed that the monolayer GaSe dominates the CBM with Ga 4p and Se 3p states in Figure 5.3(b). Furthermore, the C_2N sheet band edges were dominated by C 2p and N 2p states in Figure 5.3(a). In Figure 5.3(c), the GaSe/C_2N heterostructure showed that C 2p and N 2p states dominated the CBM, while the VBM was dominated by Ga 4p and Se 3p states.

5.3.3 Work function

Work function (Φ) is considered as one of the crucial parameters used to assess the improvement of photovoltaic performance and power conversion efficiency of GaSe/C_2N vdW heterostructure. The origin of photo-excited electrons transfer in GaSe/C_2N vdW heterostructure was plotted by aligning the Fermi energy level relative to the vacuum energy level as shown in Figure 5.4.

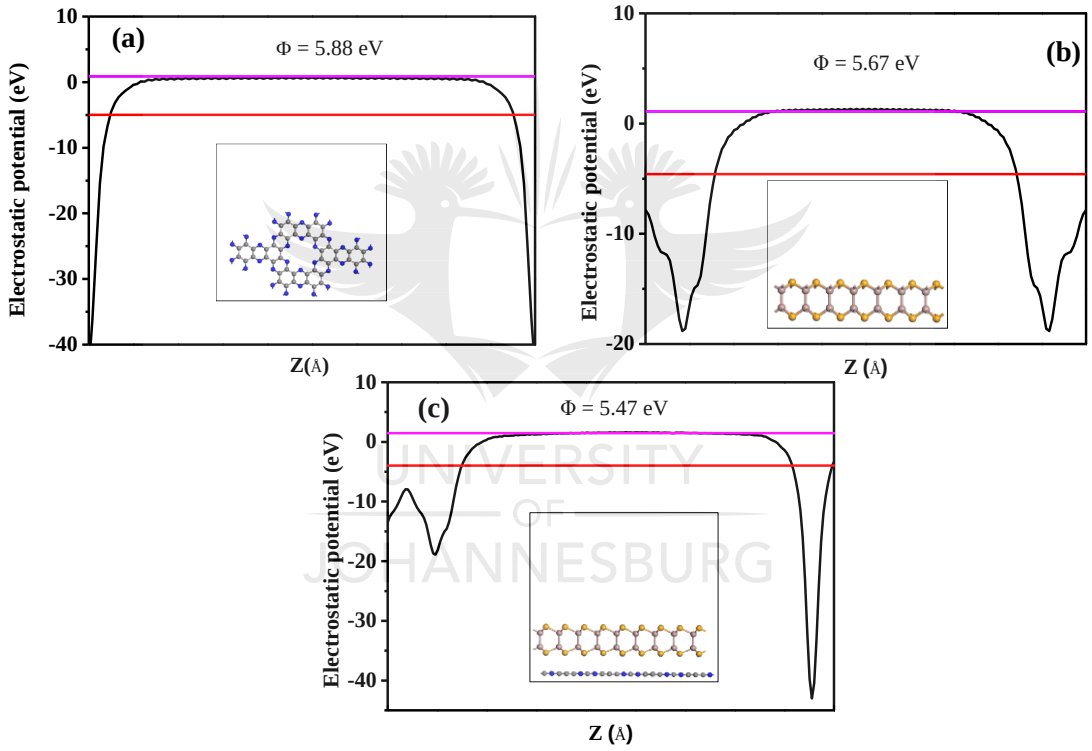

Figure 5.4. Work function for (a) C_2N sheet, (b) GaSe monolayer and (c) GaSe/C_2N vdW heterostructure.

Figure 5.4. displays the calculated work function of C_2N sheet, GaSe monolayer and GaSe/C_2N vdW heterostructure to be 5.88, 5.67 and 5.47 eV, respectively. The work function difference of the current work is about 0.3 eV compared with the previously

calculated work function of C_2N sheet of 6.18 eV by Xu *et al*. [29]. The obtained results showed that C_2N sheet has a higher work function than GaSe monolayer, which signified that the charge carriers would rather move from GaSe monolayer to C_2N sheet surface as less energy would be required for electrons to be projected from the ground state of GaSe monolayer. Therefore, in this case, GaSe monolayer would act as a positively charged semiconductor. While the C_2N sheet could serve as a negatively charged semiconductor because of the electrostatic induction. The lower ionization energy of the Se-atoms (941 kJ/mol) [30] as compared to the N-atoms (1400 kJ/mol) [31] is one of the contributing factors of the transfer of an electron from GaSe monolayer to C_2N sheet.

The calculated work function of GaSe/C_2N vdW heterostructure was reduced compared to the individual semiconductors (C_2N sheet and GaSe monolayer) with a value of 5.47 eV due to the reduced bandgap and the transfer of energized photoelectrons [32]. Moreover, GaSe/C_2N vdW heterostructure consists of electrostatic potential difference at the interface that greatly reduces the recombination rate of photogenerated electron-hole pairs, consequently increasing the transfer of charge carriers and separation.

5.3.4 Charge density differences

The difference in the bandgap structure of GaSe/C_2N van der Waals heterostructure indicates an effect of charge transfer. The charge density and delocalizations could be strongly ionized by the atomic interaction. A three-dimensional (3D) charge density difference coefficient was explored to understand the detail charge transfer at GaSe/C_2N vdW heterostructure interface, see Figure 5.5.

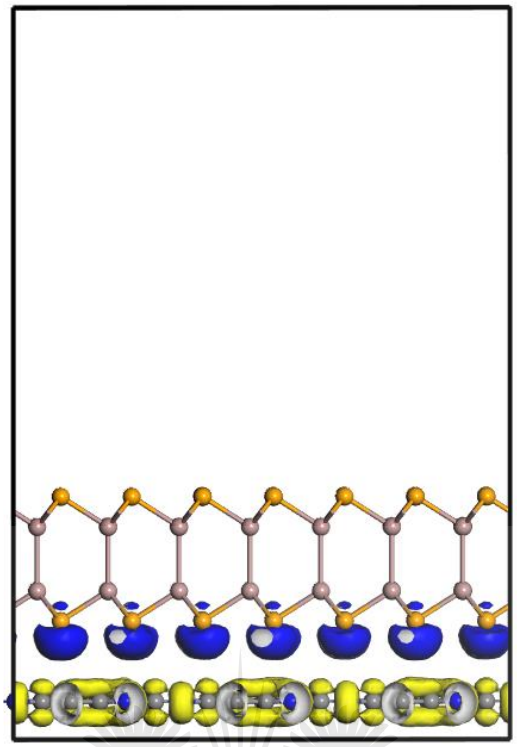

Figure 5.5. A three-dimensional (3D) charge density difference of GaSe/C_2N vdW heterostructure. The blue, dark grey, gold and light grey represent the N, C, Se and Ga atoms, respectively. The blue and yellow isosurface represents charge accumulation and depletion, respectively. The isovalue of 0.006 e Å^{-3} was set.

Figure 5.5 displays the isosurface of the charge density distribution, showing the charge delocalisation from the GaSe monolayer accumulating on the C_2N sheet, making GaSe monolayer a hole-rich (positively charged) semiconductor and C_2N sheet an electron-rich (negatively charged) semiconductor. The delocalization of charge carrier from GaSe monolayer was due to the chemically passivated and defect-free surface [33].

The photo-excited electron-hole pairs of GaSe/C_2N heterostructure is well separated so that the electrons would be transferred to the C_2N sheet and the holes

are generated in the GaSe monolayer. In the GaSe/C_2N vdW heterostructure, the recombination rate of electron-hole pairs could significantly be reduced with an improved quantum efficiency of photovoltaic applications due to the efficient charge density separation and mobility from the GaSe monolayer to C_2N sheet.

The Mulliken charge population analysis was used to quantify the amount of charge transferred within GaSe/C_2N heterostructure. A total charge of 0.10 |e| was transferred at GaSe/C_2N vdW heterostructure interface, where selenium atoms have a total average contribution of about -0.44 |e|. The total contribution of the GaSe monolayer was about -0.04 |e|. In contrast with the C_2N sheet, which received a total amount of 0.10 |e|, whereas N received more electrons than carbon atom with an average of about -0.22 |e|. This showed that the coupled GaSe monolayer loses electrons and contributes them to the C_2N sheet, thereby increasing the charge carrier transfer due to the interface distance of 3.25 Å between the GaSe monolayer and C_2N sheet. The interface could adjust the electrostatic potential to improve the detection and harvesting of solar energy. This indicates that a strong orbital overlap could be achieved, resulting in a highly efficient electron transfer for photovoltaic performance.

5.3.5 Optical properties

Generally, the visible light region plays an essential part in influencing the photovoltaic activity of the formed GaSe/C_2N heterostructure. To explore the effect of reduced bandgap on the visible light absorption of GaSe/C_2N vdW heterostructure, the optical properties calculations were performed. The UV-visible absorption spectra of C_2N sheet, GaSe/C_2N vdW heterostructure GaSe monolayer are shown in Figure 5.6.

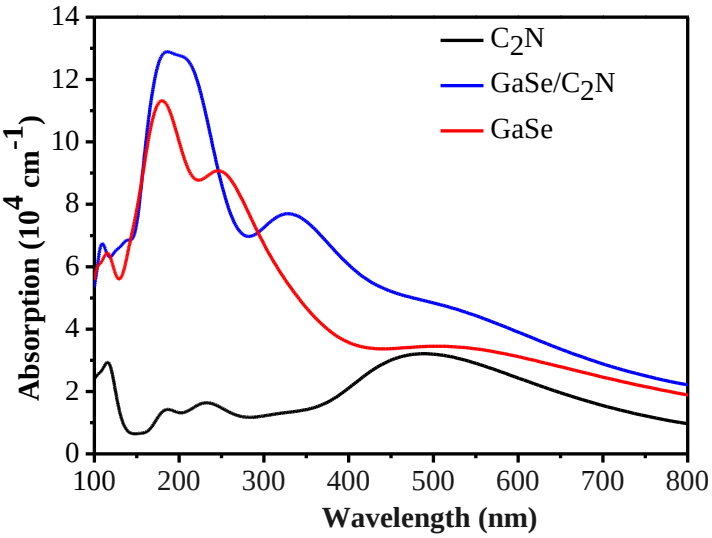

Figure 5.6. Calculated absorption spectra of pure C_2N sheet, GaSe monolayer and GaSe/C_2N vdW heterostructure.

The GaSe/C_2N vdW heterostructure shows a very high UV-visible absorption compared to the isolated C_2N sheet and GaSe monolayer. This is because GaSe/C_2N vdW heterostructure has shown a lower electronic bandgap than both C_2N sheet and GaSe monolayer. This makes the charge carriers require more energy to fill up the conduction band of both C_2N sheet and GaSe monolayer. Furthermore, GaSe/C_2N vdW heterostructure performs very well under the visible light region.

The GaSe/C_2N vdW heterostructure exhibited a broader absorption of the visible light region from 380-720 nm. The reduced suitable direct electronic bandgap and less work function electronic bandgap of GaSe/C_2N vdW heterostructure attributes to the improved UV-visible light absorption range. In summary, GaSe monolayer possesses a significant impact in reducing the bandgap of C_2N sheet, thus

enhancing the optical absorption of GaSe/C_2N vdW heterostructure in the visible range.

5.4 Band alignment mechanism

To understand the involvement of photo-excited charge carriers on the recombination, the band alignment mechanism of GaSe/C_2N vdW heterostructure was calculated. The E_{VBM} and E_{CBM} for GaSe monolayer were calculated as 0.87 and -1.19 eV, respectively, and those of C_2N layer was 0.99 and -0.97 eV, respectively. Based on the resulting band positions, a probable mechanism for the photovoltaic performance of GaSe/C_2N vdW heterostructure was proposed in Figure 5.7.

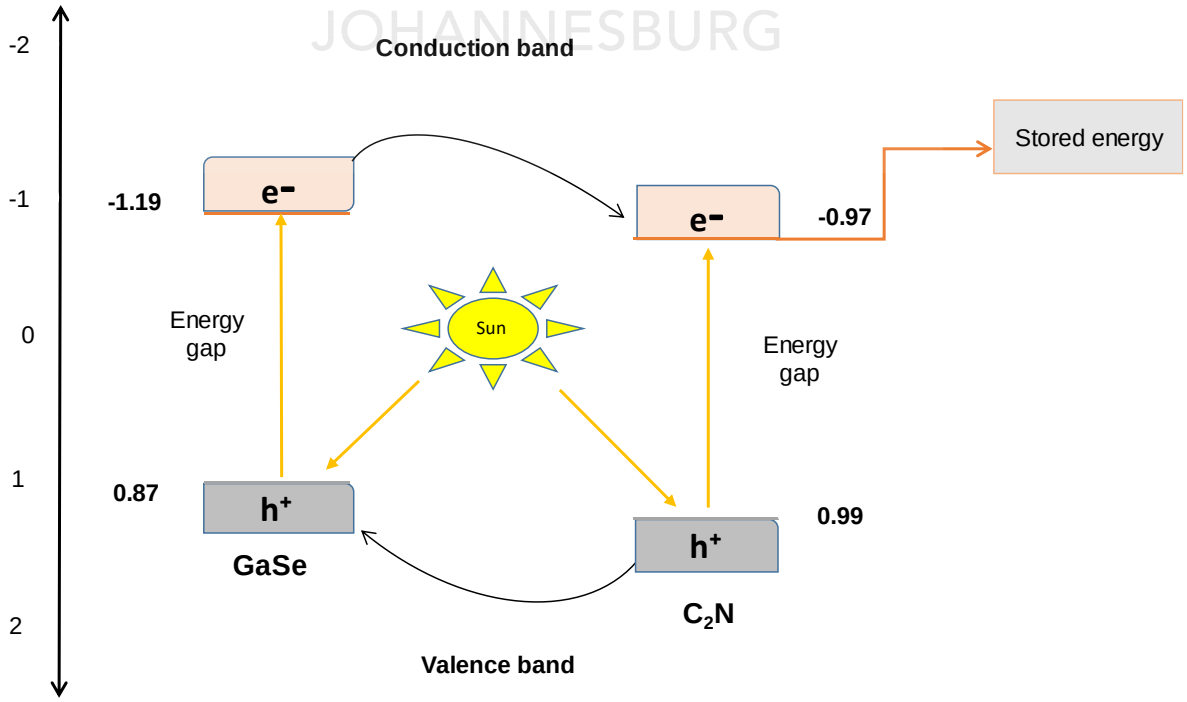

Figure 5.7. Proposed band alignment showing the type-II formation of photogenerated charge carriers in the conduction and valence bands of C_2N sheet and GaSe monolayer.

When the GaSe/C_2N vdW heterostructure is irradiated by visible light, electron-hole pairs were photogenerated in the CB and VB of C_2N sheet and GaSe monolayer. In the formation of type-II band alignment, the positioning of the conduction band and valence band of GaSe monolayer were both higher than those of the C_2N sheet. The chemical potential difference between the C_2N sheet and GaSe monolayer induces band bending at the intersection interface [34].

The band bending is the local changes in the energy offset of GaSe/C_2N vdW heterostructure band near a junction, due to space charge effects. The band bending could influence the photogenerated electrons and holes to be transferred in the opposite direction, resulting in spatial separation of electrons and holes of the GaSe/C_2N vdW heterostructure. This reduces the electrons and holes recombination making it a promising candidate to harvest visible light [35]. This suggests that the proposed GaSe/C_2N vdW heterostructure could exhibit a better separation of electrons and improve the performance of photovoltaic devices.

5.5 Conclusion

Based on the negative binding energy, the proposed GaSe/C_2N heterostructure was stabilized and could promote electrons transfer from GaSe monolayer to C_2N sheet. The obtained electronic band structure of GaSe/C_2N vdW heterostructure showed a reduced direct bandgap of 1.357 eV compared to the bandgap energy of the C_2N sheet (1.953 eV) and GaSe monolayer (2.050 eV); this was in photovoltaic cells

bandgap range. The C_2N sheet and GaSe monolayer showed a work function of 5.88 eV and 5.67 eV, respectively. Furthermore, GaSe/C_2N vdW heterostructure showed a low work function of 5.47 eV, which promotes charge transfer. The charge density distribution indicated electrons depletion on the GaSe monolayer and electrons accumulation on the C_2N sheet. The GaSe/C_2N vdW heterostructure displays an improved absorption intensity than the GaSe monolayer and C_2N sheet within the visible spectrum region of 380-740 nm. Moreover, the band alignment of GaSe/C_2N vdW heterostructure showed a type-II alignment, which assists in the reduction of the recombination rate of electron-hole pairs and thus favours the transfer of charge carriers. PCE of GaSe/C_2N vdW heterostructure was calculated to be about 21.2%, making it an appropriate fabric within the photovoltaic application.

5.6 References

[1] P. I. Hancevic, H. M. Nuñez and J. Rosellón. Distributed photovoltaic power generation: Possibilities, benefits, and challenges for a widespread application in the Mexican residential sector. *Energy Policy* **110** (2017) 478-489.

[2] K. Zweibel. Thin-film PV manufacturing: Materials costs and their optimization. *Sol. Energy Mater. Sol. Cells* **63** (2000) 375-386.

[3] K. L. Anaya and M. G. Pollitt. Going smarter in the connection of distributed generation. *Energy Policy* **105** (2017) 608-617.

[4] Y. He, Y. Pang, X. Li and M. Zhang. Dynamic subsidy model of photovoltaic distributed generation in China. *Renewable Energy* **118** (2018) 555-564.

[5] J. Yang, X. Li, W. Peng, F. Wagner and D. L. Mauzerall. Climate, air quality and human health benefits of various solar photovoltaic deployment scenarios in China in 2030. *Environ. Res. Lett.* **13** (2018) 64002-64013.

[6] G.-l. Luo, C.-f. Long, X. Wei and W.-j. Tang. Financing risks involved in distributed PV power generation in China and analysis of countermeasures. *Renewable Sustainable Energy Rev.* **63** (2016) 93-101.

[7] A. S. Brouwer, M. van den Broek, Ö. Özdemir, P. Koutstaal and A. Faaij. Business case uncertainty of power plants in future energy systems with wind power. *Energy Policy* **89** (2016) 237-256.

[8] W. Geng, L. Zhang, Y.-N. Zhang, W.-M. Lau and L.-M. Liu. First-principles study of lead iodide perovskite tetragonal and orthorhombic phases for photovoltaics. *J. Phys. Chem. C* **118** (2014) 19565-19571.

[9] S. De Wolf, J. Holovsky, S.-J. Moon, P. Löper, B. Niesen, M. Ledinsky, F.-J. Haug, J.-H. Yum and C. Ballif. Organometallic halide perovskites: sharp

optical absorption edge and its relation to photovoltaic performance. *J. Phys. Chem. Lett.* **5** (2014) 1035-1039.

[10] P.-P. Sun, Q.-S. Li, S. Feng and Z.-S. Li. Mixed Ge/Pb perovskite light absorbers with an ascendant efficiency explored from theoretical view. *Phys. Chem. Chem. Phys.* **18** (2016) 14408-14418.

[11] M. Kaltenbrunner, G. Adam, E. D. Głowacki, M. Drack, R. Schwödiauer, L. Leonat, D. H. Apaydin, H. Groiss, M. C. Scharber and M. S. White. Flexible high power-per-weight perovskite solar cells with chromium oxide–metal contacts for improved stability in air. *Nat. Mater.* **14** (2015) 1032-1039.

[12] M. Makaremi, S. Grixti, K. T. Butler, G. A. Ozin and C. V. Singh. Band engineering of carbon nitride monolayers by N-type, P-type, and isoelectronic doping for photocatalytic applications. *ACS Appl. Mater. Interfaces* **10** (2018) 11143-11151.

[13] J. Fu, J. Yu, C. Jiang and B. Cheng. g-C_3N_4-Based heterostructured photocatalysts. *Adv. Energy Mater.* **8** (2018) 1701503.

[14] D. Liang, T. Jing, Y. Ma, J. Hao, G. Sun and M. Deng. Photocatalytic properties of g-C_6N_6/g-C_3N_4 heterostructure: a theoretical study. *J. Phys. Chem. C* **120** (2016) 24023-24029.

[15] J. Li, Z. Chen, H. Yang, Z. Yi, X. Chen, W. Yao, T. Duan, P. Wu, G. Li and Y. Yi. Tunable broadband solar energy absorber based on monolayer transition metal dichalcogenides materials using Au nanocubes. *Nanomaterials* **10** (2020) 257-269.

[16] X. Qian, J. Liu, L. Fu and J. Li. Quantum spin Hall effect in two-dimensional transition metal dichalcogenides. *Science* **346** (2014) 1344-1347.

[17] C. Hu, Y. Xiao, Y. Zou and L. Dai. Carbon-based metal-free electrocatalysis for energy conversion, energy storage, and environmental protection. *Electrochem. Energy Rev.* **1** (2018) 84-112.

[18] J. Mahmood, E. K. Lee, M. Jung, D. Shin, I.-Y. Jeon, S.-M. Jung, H.-J. Choi, J.-M. Seo, S.-Y. Bae and S.-D. Sohn. Nitrogenated holey two-dimensional structures. *Nat. Commun.* **6** (2015) 1-7.

[19] A. Goetzberger, J. Luther and G. Willeke. Solar cells: past, present, future. *Sol. Energy Mater. Sol. Cells* **74** (2002) 1-11.

[20] X.-Z. Deng, Q.-Q. Zhao, Y.-Q. Zhao and M.-Q. Cai. Theoretical study on photoelectric properties of lead-free mixed inorganic perovskite RbGe1-xSnxI3. *Curr. Appl. Phys.* **19** (2019) 279-284.

[21] M. Ashwin Kishore and P. Ravindran. Tailoring the electronic band gap and band edge positions in the C_2N monolayer by P and As substitution for photocatalytic water splitting. *J. Phys. Chem. C* **121** (2017) 22216-22224.

[22] M. A. Kishore and P. Ravindran. Enhanced photocatalytic water splitting in a C_2N monolayer by C-site isoelectronic substitution. *Chem. Phys. Chem.* **18** (2017) 1526-1532.

[23] Z. Guan and S. Ni. Insights from first principles graphene/gC_2N bilayer: gap opening, enhanced visible light response and electrical field tuning band structure. *Appl. Phys. A* **123** (2017) 678.

[24] N. Wang, D. Cao, J. Wang, P. Liang, X. Chen and H. Shu. Semiconducting edges and flake-shape evolution of monolayer GaSe: role of edge reconstructions. *Nanoscale* **10** (2018) 12133-12140.

[25] J. Sun, R. Zhang, X. Li and J. Yang. A many-body GW+ BSE investigation of electronic and optical properties of C_2N. *Appl. Phys. Lett.* **109** (2016) 133108-133121.

[26] A. S. Chan, X. Fu, G. N. Panin, H. D. Cho, D. J. Lee and T. W. Kang. Shear Exfoliation and Photoresponse of 2D-Layered Gallium Selenide Nanosheets. *Physica Status Solidi (RRL)–Rapid Res. Lett.* **12** (2018) 1800226-1800230.

[27] W. Shockley and H. J. Queisser. Detailed balance limit of efficiency of p-n junction solar cells. *J. Appl. Phys.* **32** (1961) 510-519.

[28] K. Ghatak, K. N. Kang, E.-H. Yang and D. Datta. Controlled edge dependent stacking of WS_2-WS_2 Homo-and WS_2-WSe_2 Heterostructures: A Computational Study. *Sci. Rep.* **10** (2020) 1-11.

[29] W. Xu, C. Chen, C. Tang, Y. Li and L. Xu. Design of Boron Doped C_2N-C_3N Coplanar Conjugated Heterostructure for Efficient HER Electrocatalysis. *Sci. Rep.* **8** (2018) 1-9.

[30] T. Delgado, J. A. Pereira, S. Casal and E. Ramalhosa. Bioactive compounds of chestnuts as health promoters. *Nat. Bioact. Compd. Fruits Veg. Health Promoters Part II* (2016) 132-158.

[31] J. Barrett. Atomic structure and periodicity. *R. Soc. Chem.*, (2002)

[32] F. Opoku, K. K. Govender, C. G. C. E. van Sittert and P. P. Govender. Hybrid DFT study of MWCNT/Zr-doped $SrTiO_3$ heterostructure: Hydrogen production, electronic properties and charge Carrier mediator role of Zr^{4+} ion. *Int. J. Hydrogen Energy* **43** (2018) 22253-22264.

[33] S. Yang, Q. Yue, H. Cai, K. Wu, C. Jiang and S. Tongay. Highly efficient gas molecule-tunable few-layer GaSe phototransistors. *J. Mater. Chem. C* **4** (2016) 248-253.

[34] Y. Wang, Q. Wang, X. Zhan, F. Wang, M. Safdar and J. He. Visible light driven type II heterostructures and their enhanced photocatalysis properties: a review. *Nanoscale* **5** (2013) 8326-8339.

[35] Y. Liu, S. Liu, T. Wu, H. Lin and X. Zhang. Facile preparation of flower-like Bi_2WO_6/CdS heterostructured photocatalyst with enhanced visible-light-driven photocatalytic activity for Cr (VI) reduction. *J. Sol-Gel Sci. Technol.* **83** (2017) 315-323.

CHAPTER 6:

Conclusion and Recommendations

6.1 Conclusion

The purpose of this study was to investigate the theoretical aspect of GaS/C_2N and $GaSe/C_2N$ vdW heterostructures for improving their absorption of visible light activity in photovoltaic cells with high power conversion efficiency for electricity. The simulations were done by Density Functional Theory (DFT) and criteria such as work function, optical properties, photogenerated charge transfer, electronic bandgap and the geometrical structure were calculated. The following conclusions were made based on the obtained results:

- The proposed GaS/C_2N and $GaSe/C_2N$ heterostructures were formed by van der Waals interactions with enhanced photogenerated charge carrier transfer.
- The obtained bandgaps of 1.251 eV for GaS/C_2N and 1.357 eV for $GaSe/C_2N$ heterostructures were reduced compared to individual structures. This could improve the efficiency of photovoltaic cells.
- The work functions of 5.65 eV for GaS/C_2N heterostructure and 5.47 eV for $GaSe/C_2N$ heterostructure were lower than those of the individual semiconductors and this indicated that less energy is required for electron-hole pairs.
- The GaS/C_2N and $GaSe/C_2N$ heterostructures demonstrated broader visible light absorption (380-720 nm).

- The PDOS showed that orbital contributions in GaS/C_2N heterostructure were formed. The conduction band minimum (CBM) was contributed by C 2p and N 2p, while the valence band minimum (VBM) were contributed by Ga 4p and S 2p. In the GaSe/C_2N heterostructure, the VBM was contributed by Ga 4p and Se 4p, while the CBM was contributed by C 2p and N 2p.
- The calculated band edges of GaS/C_2N heterostructure exhibited type-I alignment, while GaSe/C_2N heterostructures exhibited type-II band alignments.
- The charge density difference revealed the accumulation in the C_2N sheet in both heterostructures and depletion of electrons in the GaS monolayer and GaSe monolayer, which could enhance the transfer of charge carriers.
- The power conversion efficiency (PCE) of the GaS/C_2N heterostructure was found to be 17.8% and GaSe/C_2N heterostructure was 21.2%. The calculated PCE showed a high percentage conversion of visible light.

6.2 Recommendation

The following recommendations were provided based on the findings in this research:

- The C_2N sheet should be further incorporated with GaS and GaSe semiconductors to form bilayer and trilayer for high visible light absorption.
- Important aspects such as electric field effect should be explored for the formed heterostructures to help the understanding of the bandgap tuning and photovoltaic application.

- Experimental studies should be used to fabricate the computational designed photovoltaic materials to explore their performance in energy production.